

UC Berkeley

UC Berkeley Previously Published Works

Title

Disentangling the Effects of Vapor Pressure Deficit and Soil Water Availability on Canopy Conductance in a Seasonal Tropical Forest During the 2015 El Niño Drought

Permalink

<https://escholarship.org/uc/item/9tk4s9t6>

Journal

Journal of Geophysical Research: Atmospheres, 126(10)

ISSN

2169-897X

Authors

Fang, Yilin
Leung, L Ruby
Wolfe, Brett T
[et al.](#)

Publication Date

2021-05-27

DOI

10.1029/2021jd035004

Peer reviewed

JGR Atmospheres

RESEARCH ARTICLE

10.1029/2021JD035004

Key Points:

- Canopy conductance (G_s) sensitivity to vapor pressure deficit (VPD) was analyzed from observations using multiple methods
- Estimated G_s indicates stronger limitation by soil water stress than VPD at Barro Colorado Island during the 2015 El Niño event
- With a plant hydrodynamics scheme in Energy Exascale Earth System Model (E3SM) Land Model, variation of plant hydraulic traits has greater effects on G_s limitation than on soil moisture

Supporting Information:

Supporting Information may be found in the online version of this article.

Correspondence to:

Y. Fang,
yilin.fang@pnnl.gov

Citation:








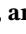


Fang, Y., Leung, L. R., Wolfe, B. T., Detto, M., Knox, R. G., McDowell, N. G., et al. (2021). Disentangling the effects of vapor pressure deficit and soil water availability on canopy conductance in a seasonal tropical forest during the 2015 El Niño drought. *Journal of Geophysical Research: Atmospheres*, 126, e2021JD035004. <https://doi.org/10.1029/2021JD035004>

Received 7 APR 2021

Accepted 23 APR 2021

© 2021. Battelle Memorial Institute. This is an open access article under the terms of the [Creative Commons Attribution License](https://creativecommons.org/licenses/by/4.0/), which permits use, distribution and reproduction in any medium, provided the original work is properly cited.

Disentangling the Effects of Vapor Pressure Deficit and Soil Water Availability on Canopy Conductance in a Seasonal Tropical Forest During the 2015 El Niño Drought

Yilin Fang¹ , L. Ruby Leung¹ , Brett T Wolfe² , Matteo Detto³ , Ryan G Knox⁴, Nate G McDowell¹ , Charlotte Grossiord⁵ , Chonggang Xu⁶ , Bradley O Christoffersen⁷ , Pierre Gentine⁸ , Charles D Koven⁴ , and Jeffrey Q Chambers⁴

¹Pacific Northwest National Laboratory, Richland, WA, USA, ²Smithsonian Tropical Research Institute, School of Renewable Natural Resources, Louisiana State University Agricultural Center, Baton Rouge, LA, USA, ³Department of Ecology and Evolutionary Biology, Princeton University, Princeton, NJ, USA, ⁴Lawrence Berkeley National Laboratory, Berkeley, CA, USA, ⁵Swiss Federal Institute for Forest, Snow and Landscape Research WSL, Birmensdorf, Switzerland, ⁶Earth and Environmental Sciences Division, Los Alamos National Laboratory, Los Alamos, NM, USA, ⁷Department of Biology, University of Texas Rio Grande Valley, Edinburg, TX, USA, ⁸Department of Earth and Environmental Engineering, Columbia University, New York, NY, USA

Abstract Water deficit in the atmosphere and soil are two key interactive factors that constrain transpiration and vegetation productivity. It is not clear which of these two factors is more important for the water and carbon flux response to drought stress in ecosystems. In this study, field data and numerical modeling were used to isolate their impact on evapotranspiration (ET) and gross primary productivity (GPP) at a tropical forest site in Barro Colorado Island (BCI), Panama, focusing on their response to the drought induced by the El Niño event of 2015–2016. Numerical simulations were performed using a plant hydrodynamic scheme (HYDRO) and a heuristic approach that ignores stomatal sensitivity to leaf water potential in the Energy Exascale Earth System Model (E3SM) Land Model (ELM). The sensitivity of canopy conductance (G_s) to vapor pressure deficit (VPD) obtained from eddy-covariance fluxes and measured sap flux shows that, at both ecosystem and plant scale, soil water stress is more important in limiting G_s than VPD at BCI during the El Niño event. The model simulations confirmed the importance of water stress limitation on G_s , but overestimated the VPD impact on G_s compared to that estimated from the observations. We also found that the predicted soil moisture is less sensitive to the diversity of plant hydraulic traits than ET and GPP. During the dry season at BCI, seasonal ET, especially soil evaporation at VPD > 0.42 kPa, simulated using HYDRO and ELM, were too strong and will require alternative parameterizations.

Plain Language Summary Plants close stomata to regulate water loss through transpiration when stressed by the dry soil or high atmospheric water demand (vapor pressure deficit, VPD) or both. Tropical forests have experienced periodic droughts in the past. Recent drought-related plant mortality has been attributed to increasing VPD associated with climate change. To evaluate whether water stress from dry soil or VPD has more limiting effect on plant transpiration, we analyzed the results from statistical models fitted to two types of field observation data and a land surface model which can simulate water movement in the soil and the water transport within the plant at a tropical forest site in Panama. We found dry soil is more important in limiting plant water loss at the site during the drought of the El Niño event of 2015–2016 and identified future model improvement need.

1. Introduction

Tropical forests play a key role in the global carbon cycle by storing atmospheric carbon, reducing the climatic impact of anthropogenic emissions (Pan et al., 2011; O. L. Phillips et al., 2009). A warmer and drier climate may weaken the ability of tropical forests to mitigate CO₂ emissions (Cavaleri et al., 2017; Corlett, 2016). A recent review on the response of tropical rainforests to drought has highlighted the complex mechanisms underlying forest vulnerability to drought (Bonafant et al., 2016). The short-term plant response to water stress is to close stomata to regulate water loss (Daszkowska-Golec & Szarejko, 2013) especially at high vapor pressure deficit (VPD) (Grossiord et al., 2020; Massmann et al., 2019; Novick et al., 2016; Oren

et al., 1999). Accurate estimation of plant transpiration reduction due to water stress is critical to the understanding of tropical forest responses to drought and improving predictions of the global water and carbon cycles (Gentine et al., 2019; Lemordant et al., 2018; Mencuccini et al., 2019). Hence understanding and modeling the combined effect of drought stress and the effect of temperature and VPD is a major research gap for improving prediction of the response of the tropical forest to severe and frequent drought conditions (Bonal et al., 2016; Green et al., 2020).

Multiple approaches have been proposed to model the stomatal response to VPD. However, in most Earth system models, plant stomatal response to water stress is heuristically related to soil water status (soil moisture or soil water potential) (Christoffersen et al., 2016; Verhoef & Egea, 2014), neglecting the important impact of atmospheric demand on leaf water potential (Eller et al., 2020; Sperry & Love, 2015). Yet, leaf water potential has been used as a measurable indicator of plant water stress (Osakabe et al., 2014; Xu et al., 2016; Zhou et al., 2013). Empirical results that consider leaf water potential, however, are still controversial. For example, Anderegg et al. (2017) improved prediction of stomatal conductance when stomatal sensitivity to declining leaf water potential during water stress was included in their simulation. In contrast, Wu et al. (2020), using leaf conductance measured in the upper canopy of 15 tropical trees in two contrasting Panamanian forests, show that the inclusion of leaf water potential did not improve model performance. Plants have a variety of morphological and physiological strategies to tolerate drought, including hydraulic strategies to use deep root systems to extract soil moisture in deeper regions so that a higher xylem pressure can be maintained during drought (Choat et al., 2018). In addition to rainfall variability, plant hydraulic traits have been found to be crucial in explaining the spatial pattern of dry tropical forest responses to water stress in Central America (Xu et al., 2016).

Inclusion of a mechanistic representation of plant hydraulics can provide an important link between soil and evaporative demand and improve the prediction of plant response to drought (Christoffersen et al., 2016; Grossiord et al., 2020; Kennedy et al., 2019; Liu et al., 2020; Sperry & Love, 2015). Motivated by notable improvements in models that link water transport to stomatal conductance, plant hydraulics have started to be physically represented in land surface models and biosphere models, such as Ecosystem Demography Model (ED2) (Xu et al., 2016), CLM5 (Kennedy et al., 2019), a tractable land surface model (Sabot et al., 2020), the Joint UK Land Environment Simulator (JULES) (Eller et al., 2020), LM3PPA-TV (Cano et al., 2020), and Noah-MP (Li et al., 2021). Recently, a plant hydrodynamics (HYDRO) model (Christoffersen et al., 2016) has been implemented in the Functionally Assembled Terrestrial Ecosystem Simulator (FATES) (Fisher et al., 2018), which is a dynamic vegetation module that is currently coupled to CLM and the land model (ELM) of Energy Exascale Earth System Model (E3SM) (Golaz et al., 2019; Leung et al., 2020).

It has become an emerging research topic whether atmospheric moisture stress is a dominant limitation for vegetation productivity and water use during periods of hydrologic stress (Liu et al., 2020; Massmann et al., 2019; Novick et al., 2016; Sulman et al., 2016; Yuan et al., 2019) as concurrent drought (soil water stress) and high atmospheric water deficit (VPD) often co-occur (Zhou et al., 2019). These two interactive factors both constrain transpiration and vegetation productivity and they should be accounted for together to explain changes in ecosystem fluxes (Stocker et al., 2019; and references therein). Yet few studies using land-surface models have separately resolved the response of plant functioning to high VPD and soil water stress. This can limit model predictability of future climate impacts on terrestrial ecosystems (Grossiord et al., 2020). In this study, we use a numerical model that represents plant hydraulics and observation data analysis to disentangle the importance of VPD and soil water stress on canopy conductance (G_s) at a tropical forest site in Barro Colorado Island (BCI), Panama during the 2015–2016 El Niño–Southern Oscillation (ENSO) event. The goals of this study are to improve understanding of tropical forest responses to drought and to inform experiments and observational studies for new data collection, as well as new model development needs.

2. Methods

2.1. Model Description

The E3SM land model version 1 (ELMv1) for this study is identical to the Community Land Model version 4.5 (Oleson et al., 2013) in most aspects except for some biogeochemistry components (Burrows et al., 2020;

Ricciuto et al. 2018), which are not turned on in this study. As in CLM4.5, stomatal conductance in the standard ELM version is heuristically related to soil water stress (Oleson et al., 2013):

$$\beta = \sum_i \frac{\psi_C - \psi_{S,i}}{\psi_C - \psi_O} r_i \quad (1)$$

where β is the stress factor, $\psi_{S,i}$ is the soil water matric potential of layer i (m), ψ_C is the soil water potential (m) when stomata are fully closed, ψ_O is the soil water potential (m) when stomata are fully open, and r_i is the root fraction in soil layer i . β ranges from 0 to 1. $\beta = 1$ when vegetation is not water stressed. This stress factor only relies on soil water potential and it does not represent plant adaptation to available water (Mencuccini et al., 2019; Sabot et al., 2020; Xu et al., 2016; and references therein).

Evapotranspiration (ET) is calculated as water extraction by roots from each soil layer, and the fraction of root uptake of water from soil layer i follows Equation 2:

$$r_{e,i} = \left(\frac{\psi_C - \psi_{S,i}}{\psi_C - \psi_O} r_i \right) \frac{1}{\beta} \quad (2)$$

where $r_{e,i}$ is the effective root fraction. Transpiration multiplied by $r_{e,i}$ for each soil layer represents the local sink term (extracted from the soil) in the soil hydrology model. In this model, water transport within the roots is not simulated.

In order to overcome some of the limitations of the heuristic approach and explore mechanistically the role of plant hydraulics, we used a plant hydrodynamics scheme (HYDRO), which is an extension of the model described in Christoffersen et al. (2016). HYDRO is a standalone module that can be coupled with any host land models via a user interface. HYDRO simulates the water transport through different organs in the plants, from roots to leaves, taking into account the plant internal water storage that can buffer the imbalance of root water uptake and transpiration demand (Bartlett et al., 2019; Huang et al., 2017; N. G. Phillips et al., 2003; Pineda-Garcia et al., 2013; Tian et al., 2018). The model schematic is shown in Figure 1. An individual tree is divided into four porous media: leaf, stem, transporting root (trout), and absorbing root (aroot). Except for the absorbing root, which is divided into compartments for each soil layer, the other types are each represented by single compartments. The soil in each layer is radially discretized into cylindrical shells representing the rhizosphere around an absorbing root (Figure 1).

The transient water mass balance equation in one dimension along the hydraulic path for each compartment i can be written as:

$$\rho_w V_i \frac{d\theta_i}{dt} = -Q_{i-1} + Q_i \quad (3)$$

The mass flux in each section is based on the length integral of Darcy's law:

$$Q_i = -K_i (\psi_{i-1} - \psi_i + \rho_w g (z_{i-1} - z_i)) \quad (4)$$

in which i is the compartment number starting from the leaf compartment toward the outermost soil shell, ρ_w is the density of water (kg m^{-3}), V_i is the volume of modeled compartment (m^3), θ_i is the soil volumetric water content ($\text{m}^{-3} \text{m}^{-3}$). Plant tissue water storage capacity can increase water accessibility for transpiration and buffer dry period water supply (Hartzell et al., 2017), Q_i (kg s^{-1}) is the water mass flux between compartments i and $i+1$ (positive for movement toward the leaf), g is acceleration due to gravity ($=9.81 \text{ m s}^{-2}$) and ψ_i is xylem or soil matric water potential (MPa), t is time (s), z_i is the elevation above (positive) or below (negative) the ground (m), and K_i is the conductance ($\text{kg MPa}^{-1} \text{ s}^{-1}$) at the boundary between compartment i and $i+1$. K_i is calculated using the following equation:

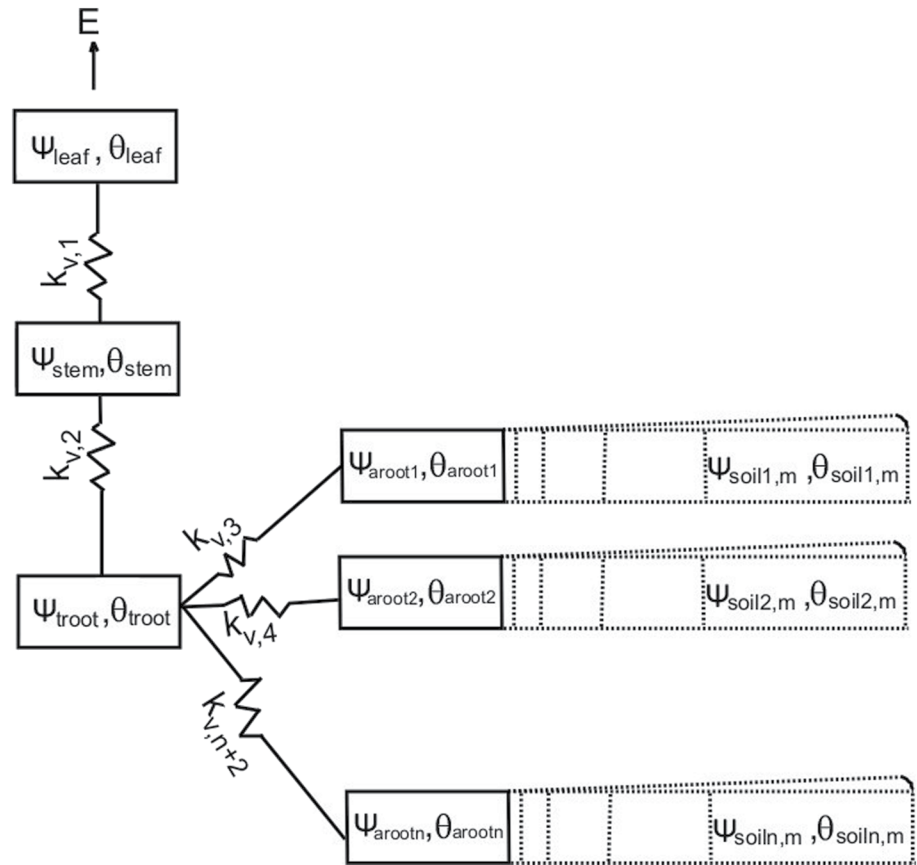


Figure 1. Schematic of the plant hydrodynamics scheme, HYDRO.

$$K_i = \left\{ \begin{array}{ll} K_{max,i} k_{r,i} & i \in \text{other boundaries} \\ \left[\frac{1}{K_{max,aroot} k_{r,aroot}} + \frac{1}{K_{max,shell} k_{r,shell1}} \right]^{-1} & i \in \text{boundary shared by aroot and soil shell} \end{array} \right\} \quad (5)$$

where k_r is the relative hydraulic conductance (dimensionless), $K_{max,i}$ is the maximum conductance ($\text{kg MPa}^{-1} \text{s}^{-1}$) at the boundary, $K_{max,aroot}$ is the maximum conductance ($\text{kg MPa}^{-1} \text{s}^{-1}$) of the absorbing root, $K_{max,shell1}$ ($\text{kg MPa}^{-1} \text{s}^{-1}$) is the maximum conductance of the soil shell (*shell1*) next to the absorbing root, $k_{r,aroot}$ and $k_{r,shell1}$ are relative conductance (dimensionless) for the absorbing root and shell1 (nearest shell to the root), respectively. k_r i 's at the compartment boundaries shared by the absorbing root and soil shell are estimated by the harmonic mean method, k_r i 's at the other boundaries are estimated using the upstream weighting method, i.e., they are chosen in relation with the direction of flow (Haverkamp & Vauclin, 1979). $K_{max,i}$ incorporates not only the inherent plant tissue or soil conductivity per unit volume ($k_{max,i}$; $\text{kg MPa}^{-1} \text{m}^{-1} \text{s}^{-1}$), but also sapwood area, the path length, and a correction factor for xylem conduit taper as described in Christoffersen et al. (2016).

The relationship between water potential ψ_i and the relative water content $s_{i,i}$ (water content θ_i relative to the maximum water content or porosity θ_{sat} on a per volume basis) comprises three successive regions, i.e., a capillary region, an elastic drainage region, and embolism region. In each plant compartment, the water potential is described using pressure-volume (PV) curves given by the following equations:

$$\psi_i(\theta_i) = \begin{cases} \psi_0 - m_{cap} \left(1 - \frac{\theta_i}{\theta_{sat}}\right) & s_{ft,i} \leq s_{l,i} \leq 1 \\ \psi_{sol,i}(\theta_i) + \psi_{p,i}(\theta_i) & s_{tlp,i} \leq s_{l,i} \leq s_{ft,i} \\ \psi_{sol,i}(\theta_i) & s_{r,i} \leq s_{l,i} < s_{tlp,i} \end{cases} \quad (6)$$

From the top to the bottom, the three equations in Equation 6 describe three successive dehydration phases: a capillary drainage region, followed by an elastic drainage region, and then a final embolism region. These regions distinguish the locations that are responsible for the release of plant water storage (Christoffersen et al., 2016; Steppe, 2018). Capillary region represents the release of sapwood capillary water storage. In the elastic region, elastic water stored within living cells is released, and water is released in the embolism region when air replaces the water-filled volume. m_{cap} is the slope for the linear drainage of capillary water, ψ_0 is the saturated water potential (MPa). $\psi_{sol,i}$ is the solute potential (or osmotic potential) (MPa) (<0) caused by the presence of solutes in living cells, $\psi_{p,i}$ is the pressure potential or cell wall turgor pressure (MPa), which is normally positive or zero, $s_{ft,i}$ is the relative water content at which elastic drainage begins, $s_{tlp,i}$ is the relative water content corresponding to the turgor loss point (TLP), $s_{r,i}$ is the residual relative water content. ψ_{sol} and ψ_p are given by:

$$\psi_{sol}(s_l) = -\frac{|\pi_0|(s_{ft} - s_r)}{s_l - s_r} \quad (7)$$

$$\psi_p(s_l) = |\pi_0| - \varepsilon \left(\frac{s_{ft} - s_l}{s_{ft} - s_r} \right) \quad (8)$$

where π_0 (MPa) is osmotic potential at full turgor, and ε (MPa) is the bulk elastic modulus which describes the flexibility of plant tissues, which is defined as the ratio of the change in cell turgor to change in the relative leaf cell volume (Saito et al., 2006).

The xylem vulnerability curve in every compartment follows:

$$k_{r,i} = \left[1 + \left(\frac{\psi_i}{P_{50,i}} \right)^{a_i} \right]^{-1} \quad (9)$$

The soil water characteristic curve is described using the Clapp & Hornberger empirical equations (Clapp & Hornberger, 1978) in Equations 10 and 11:

$$s_{l,i} = \left(\frac{\psi_i}{\psi_b} \right)^{-\lambda} \quad (10)$$

$$k_{r,i} = \left(\frac{\psi_i}{\psi_b} \right)^{-2-3\lambda} \quad (11)$$

where $P_{50,i}$ is the water potential (MPa) at which 50% of maximum conductance is lost and a_i is a shape index (dimensionless), λ is pore size distribution index (dimensionless), ψ_b is the air entry pressure head (MPa).

The boundary conditions are the transpiration mass flux (kg s^{-1}), and zero-flux for the outermost rhizosphere element. Calculation of the hydraulic impacts on stomatal conductance g_s ($\mu\text{mol H}_2\text{O m}^{-2} \text{s}^{-1}$), is empirically related to the leaf water potential ψ_l (MPa), following Christoffersen et al. (2016):

$$g_s = g_{s,max} \times \beta(\psi_l) \quad (12)$$

where $g_{s,max}$ is the maximum stomatal conductance ($\mu\text{mol H}_2\text{O m}^{-2} \text{s}^{-1}$) in the absence of water supply limitation as given by the Ball-Berry stomatal conductance model (Collatz et al., 1991) in ELM, and β is a water stress fraction that depends on leaf water potential according to Equation 13 which replaces Equation 1,

$$\beta = \left[1 + \left(\frac{\psi_l}{P_{50,gs}} \right)^{a_{gs}} \right]^{-1} \quad (13)$$

where $P_{50,gs}$ is the leaf water potential at 50% stomatal closure, and a_{gs} is shape parameter for stomatal control. Equation 13 has been implemented also in Xu et al. (2016) to calculate the stress factor, but TLP was used instead of $P_{50,gs}$. These two parameterizations ($P_{50,gs}$ and TLP) of Equation 13 will be included in the following sections.

The original plant hydrodynamic model developed by Christoffersen et al. (2016) for individual trees of different sizes was modified to conform to the big leaf version of ELM, using average tree height (m) to calculate the total individual tree biomass, canopy biomass, belowground biomass for each plant functional type (PFT). The number of trees n_i of the i th PFT is calculated using the following equation:

$$n_i = \frac{A_g}{sla_i} \cdot LAI \cdot \frac{wt_i}{B_{leaf,i}} \quad (14)$$

where A_g is the ground area (m^2), sla_i is the specific leaf area of the i th PFT (m^2/gC), LAI is the leaf area index (m^2/m^2), wt_i is the fraction of leaf area for the i th PFT, and $B_{leaf,i}$ is leaf biomass per individual in carbon units ($\text{gC}/\text{individual}$). With the exceptions of the stem and absorbing root compartments, the volume of each compartment is derived from the biomass pools calculated using the allometric equations specified in FATES as function of average height. The volume of the stem is the sapwood area times the tree height. The total volume of the absorbing root is calculated using a given specific root length (m g^{-1}), root biomass (g), and absorbing root radius (m). The absorbing root volume in each soil layer is a fraction of the total root length in that layer times the total volume. When HYDRO is activated, fluxes calculated based on ET fractions in Equation 2 are replaced with the water fluxes calculated from HYDRO. It can be negative or positive depending on whether soil shells lose or gain water.

For this study, the soil in each layer is radially discretized into 5 cylindrical shells around an absorbing root (Figure 1). The mass balance equations for the plant-soil system in each soil layer and compartment are solved simultaneously using the Newton-Raphson approach with water potentials as prognostic variables.

The coupling of ELM-HYDRO can be easily implemented through an application interface because HYDRO is designed such that it works as a library that can be plugged into a selection of driver land models such as CLM and ELM. ELM and HYDRO share the same soil volume. Via ELM's soil hydrology scheme, runoff, drainage, and soil water fluxes between layers are calculated given infiltration as top-boundary conditions and root water extraction calculated in HYDRO as sources/sinks. The change in water content in each soil layer is then passed back to the plant hydraulics model through the application interface in ELM. A soil layer in ELM is represented by one grid cell, while it is represented by five grid cells in HYDRO. The change in ELM soil water content is downscaled to water contents of the rhizosphere shells of the same layer following a heuristic approach. That is, in the case of a net gain in soil moisture calculated in ELM relative to the previous time step, shells in HYDRO are filled with water in order from the driest to the wettest shell, and for a net loss of soil moisture, water in soil shells are drained in order from the wettest to the driest shell. For comparison, the model that ignores plant hydrodynamics is simply referred to as ELM in the following sections, and the model that considers hydrodynamics by coupling ELM with HYDRO is simply referred to as HYDRO.

2.2. Study Sites

Our study site is located at BCI (9°10'N, 79°51'W), Panama. The 50-ha forest plot at BCI is one of the best-studied tropical forest sites in the world (Kupers et al., 2019). The wet season at BCI is roughly from May to December and the dry season is from late December to April. Meteorological data from 2003 to 2016 is available from a meteorological tower near the Lutz catchment at BCI (Faybishenko et al., 2018). BCI had a long dry season in 2016 during the strong El Niño event of 2015–16 (Detto et al., 2018). Annual mean precipitation during the simulation period is 2382.7 mm, while mean precipitation in the dry season is 219 mm. Average annual and dry season relative humidity at BCI are 88.5% and 83.5%. Mean annual and dry season temperatures are respectively 26.0°C and 26.4°C at BCI.

2.3. BCI Data set

Field efforts at BCI in the last 35 years have generated a rich set of data, such as continuous meteorological forcing, streamflow, ET, soil water potential, soil moisture content, as well as leaf water potential, sapflow, and plant hydraulic traits for trees at the higher elevation plateau of the island, more prone to water stress in drought conditions. This data set provides a unique opportunity to evaluate the plant hydraulics model and tropical forest response to drought conditions at this site.

At BCI, ET was measured by an eddy-covariance system installed on a tower, the AVA tower (~1.5 km from the Lutz catchment) located 41 m above the ground on the top plateau. The eddy-covariance system comprised a sonic anemometer (CSAT3, Campbell Scientific, Logan, UT) and an open-path infrared CO₂/H₂O gas analyzer (LI7500, LiCOR, Lincoln, NE). High-frequency (10 Hz) measurements were acquired by a datalogger (CR1000, Campbell Scientific) and stored on a local computer. Data were processed with a custom program using a standard routine described in Detto et al. (2010). Hydrometeorological variables collected on the same tower and used in the postprocessing included: air temperature, relative humidity, air pressure, radiation components, rainfall, and soil moisture. These variables were stored at 5-min interval.

Eddy-covariance fluxes were computed on a 30-minute averaging window, a de-spiking algorithm was applied to detect and remove spikes (values greater than six standard deviations in a one-minute window), values exceeding a reasonable physical range, or low diagnostic instrument values. Fluxes were corrected for air density fluctuations (Detto & Katul, 2007). A QA/QC was applied to the 30-min turbulent fluxes to remove measurement during and immediately after rain events, out of reasonable physical limits or not satisfying other turbulent criteria (Pau et al., 2018). Gaps were filled using Artificial Neural Network and hydrometeorological inputs.

Soil moisture was monitored using three Time Domain Reflectometers (TDR, CS616, Campbell Scientific) installed vertically in the vicinity of the tower in July 2012 at 0 to 15 cm depths. The TDR probes measured the apparent permittivity of soil that can be related to the soil water content using an *ad hoc* calibration curve (Kelleners et al., 2005). Seven *in situ* gravimetric soil water content samples (0–15 cm) were collected near the probes during different soil moisture regimes (30 campaigns). TDR soil water content compares well with gravimetric sampling.

Leaf water potential was measured on four canopy trees (*Inga pezizifera*, *Gustavia superba*., *Miconia argentea*, and *Simarouba amara*) during the 2016 dry season, on March 12, 2016. These trees are relatively abundant in the footprint of the eddy covariance tower. Between predawn (0600 h) and late afternoon (1,800 h), six measurements of water potential were taken (Wolfe et al., 2019). At each time, three sun exposed leaves were collected from each tree with a pruning pole or slingshot. The leaves were immediately sealed in humidified plastic bags, placed in a cooler with ice, and, within two hours, water potential was measured with a pressure chamber (PMS Instruments Albany, OR, USA). Sap flux density was measured on each of those trees with custom-built thermal dissipation probes (Granier, 1985). On each tree, two probes were placed on opposite sides of the main bole at 1.3 m height, extending 1 cm into the sapwood. Measurements were taken every 15 s and averages were recorded every 5 min on CR1000 and CR800 data loggers (Campbell Scientific). Sap flux density was calculated using the calibration of Granier (1985).

Maximum stem area-specific hydraulic conductivity (K_{max}) and vulnerability curves (Equation 9) were derived from laboratory measurements on terminal branches collected from canopy trees of each of the

Table 1
Default Hydraulic Traits Used by HYDRO in ELM

| Parameter | Leaf | Stem | trout | aroot |
|---|--------|-------|-------|-------|
| Saturated water content (θ_{sat}) (m^3/m^3) | 0.65 | 0.65 | 0.65 | 0.75 |
| Osmotic potential at full turgor (π_0) (MPa) | -1.47 | -1.23 | -1.23 | -1.04 |
| Bulk elastic modulus (ϵ) (MPa) | 12 | 10 | 10 | 8 |
| Residual saturation fraction (s_r) (-) | 0.25 | 0.325 | 0.325 | 0.15 |
| Xylem vulnerability curve shape parameter (a_i) (-) | 2 | 2 | 2 | 2 |
| Maximum xylem hydraulic conductivity (K_{max}) ($kg\ MPa^{-1}m^{-1}s^{-1}$) | - | 3.0 | - | - |
| Maximum conductivity for unit root surface ($kg\ m^{-2}\ MPa^{-1}s^{-1}$) | - | - | - | 0.003 |
| Xylem water potential at 50% loss of conductivity (P_{50}) (MPa) | -2.25 | -2.25 | -2.25 | -2.25 |
| Water potential at 50% loss of stomatal conductance (P_{50gs}) (MPa) | -1.5 | - | - | - |
| Shape parameter for stomatal control (a_{gs}) (-) | 2.5 | - | - | - |
| Leaf area per sapwood area ($A_l:A_s$) (m^2/cm^2) | 0.8 | | | |
| Specific root length (SRL) (m/g) | 25.0 | | | |
| Fraction of woody biomass that is above ground (abg_frac) (-) | 0.6 | | | |
| Fraction of total tree resistance from trout to canopy ($rfrac$) (-) | 0.625 | | | |
| Absorbing root radius (r_s) (m) | 0.0001 | | | |

Abbreviations: ELM, Energy Exascale Earth System Model (E3SM) Land Model; HYDRO, hydrodynamic.

focal species. Following Wolfe et al. (2016), stem segments were bench-dried to stem water potentials that ranged -0.15 to -6.64 MPa, then measured for hydraulic conductivity. Stem water potential was measured with psychrometers in the laboratory following Wolfe (2017). Details can be found in the data set in Wolfe et al. (2021). Vulnerability curves were fit using nonlinear quantile regression with the package *quantreg* in R. Within the regression, an intercept term was included in Equation 5 to account for raw values of K_{max} rather than assuming proportionality. K_{max} was calculated as the intercept of the regression (Figure S1).

2.4. Model Parameters and Sensitivity Experiments

Hydraulic trait parameters for HYDRO are listed in Table 1, which represent mean values observed for tropical forests based on a pantropical hydraulic traits data set synthesized by Christoffersen et al. (2016) from the literature and existing trait databases. We use a tree height of 24.9 m for trees observed at BCI for the simulations, which is reasonable as a global forest canopy height map in Lefsky (2010) shows that the 90th percentile height of tropical humid forests are greater than 20 m. The two parameters defining the root profile model adopted from Jackson et al. (1996) are $r_a = 7$, $r_b = 1$, respectively, resulting in 99% of roots in the top 4 m of soil. In ELM, the default ψ_0 and ψ_C in Equation 1 are -66 and -255 m, respectively. The average observed LAI at BCI is ~ 6.0 (Detto et al., 2018).

A total of 80 simulations were run using plant traits of a single species for the whole plot. Apart from the saturated xylem conductivity (K_{max}), water potential at which 50% of xylem conductivity is lost (P_{50}), and xylem vulnerability curve shape parameter (a) measured at BCI for the four canopy trees (*Inga peyzifera*, *Gustavia superba.*, *Miconia argentea*, and *Simarouba amara*) Table 2, we also combined 29 sets of K_{max} , P_{50} , and a_i in Barros et al. (2019), and 47 sets of K_{max} , P_{50} , TLP, wood density (WD, $g\ cm^{-3}$) and specific leaf area (SLA, $m^2\ g^{-1}$) compiled in Xu et al. (2016) for individual species. For the Barros' data, parameter a was calculated using the sigmoidal function and the water potential at which 88% of xylem conductivity is lost (P_{88}) as reported in Barros et al. (2019). For the Xu data, a_i and a_{gs} were set to 4 and 6, respectively, following the code in the supplementary information in Xu et al. (2016). Data from Xu et al. were for seasonally dry tropical forest sites and data from Barros et al. included two tropical Amazon forests with contrasting seasonal precipitation. These data (Table S1) resulted in a range of K_{max} (0.16–23.9 $kg\ MPa^{-1}m^{-1} s^{-1}$), P_{50} (-5.02 to -0.76 MPa), TLP (-3.12 to -0.69 MPa), SLA (0.00515–0.0199 $m^2\ g^{-1}$), WD (0.31–0.86 $g\ cm^{-3}$), and a (1.723–157.4) (Figure 2) and they were used to evaluate

| Species | Height (m) | DBH (cm) | K_{\max} (kg MPa ⁻¹ s ⁻¹) | P_{50} (MPa) | a (-) |
|---|------------|----------|--|----------------|--------|
| <i>Inga pezizifera</i> (Fabaceae) | 25.3 | 34.0 | 3.624 | -1.561 | 10.088 |
| <i>Gustavia superba</i> (Lecythidaceae) | 15.3 | 24.1 | 1.413 | -1.796 | 1.717 |
| <i>Miconia argentea</i> (Melastomataceae) | 17.7 | 23.9 | 6.998 | -0.597 | 0.924 |
| <i>Simarouba amara</i> (Simaroubaceae) | 21.7 | 37.4 | 3.542 | -1.071 | 4.814 |

Abbreviation: DBH, diameter at breast height.

the diversity of hydraulic traits on ET and gross primary productivity (GPP) response to VPD and soil water stress at BCI. As the model is the big leaf version, in which sub-grid tiling operates on the basis of plant functional types, we only consider the dominant broadleaf trees in our study. No biodiversity of trait sets is accounted for.

2.5. Calculation of G_s

Canopy conductance (G_s , m s⁻¹) can be calculated from the eddy covariance data and sapflux measurements as shown in the following.

2.5.1. Inversion of the Penman–Monteith (PM) Equation

Eddy-covariance data were used to calculate G_s by the following equation inverted from the PM equation (Barros et al. 2019; Novick et al., 2016; Vourlitis et al., 2008):

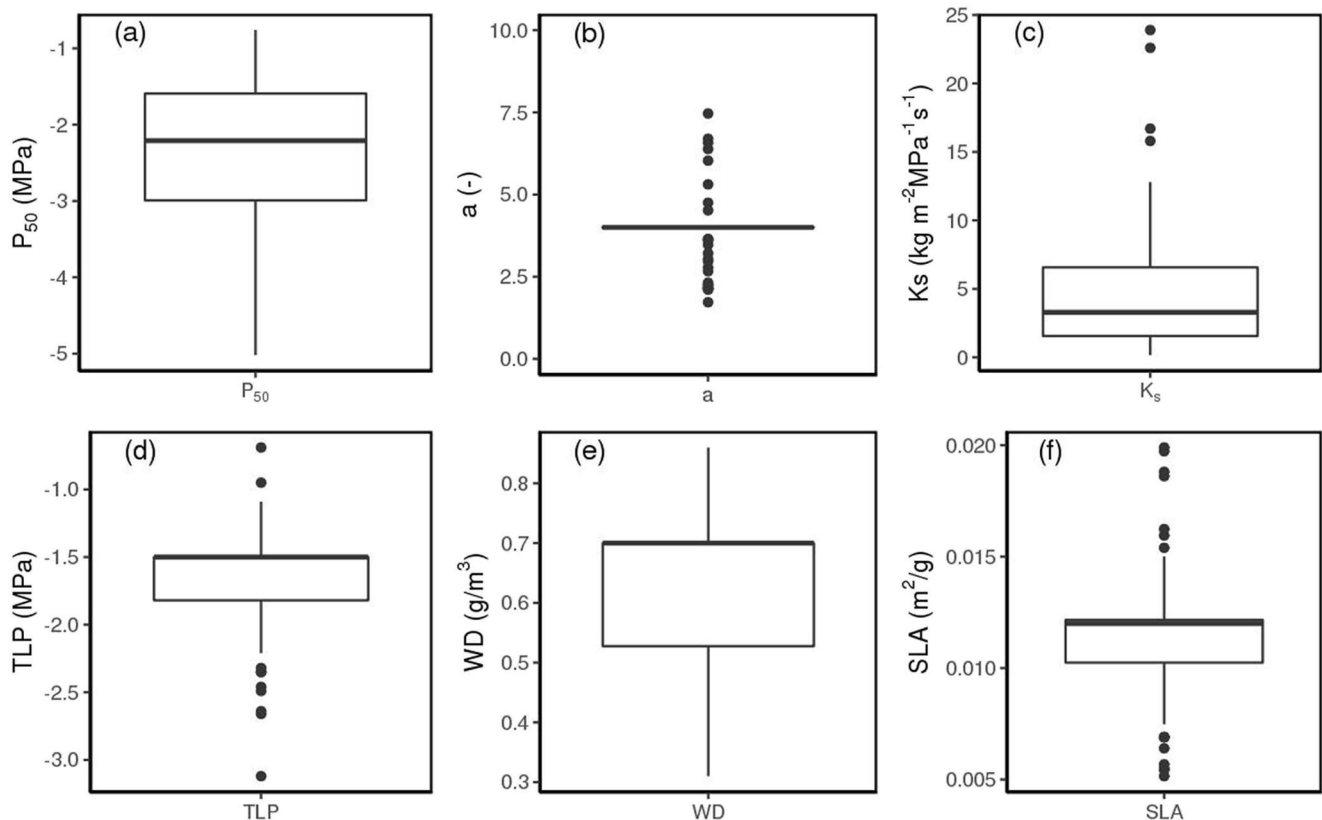


Figure 2. Box plots of P_{50} (a), a (b), K_{\max} (c), combined $P_{50,gs}$ and TLP (d), WD (e), and SLA (f) used in HYDRO simulations. SLA, specific leaf area; TLP, turgor loss point; WD, wood density.

$$G_s = \frac{G_a T \lambda \gamma}{\Delta A + \rho C_p (e_s - e_a) G_a - \lambda T (\Delta + \gamma)} \quad (15)$$

where G_s (m s⁻¹) is canopy conductance, T is the transpiration (kg m⁻² s⁻¹), λ (J kg⁻¹) is the latent heat of water vaporization, Δ is temperature-dependent slope of the saturation-vapor pressure curve, γ (Pa K⁻¹) is the psychrometric constant, A (W m⁻²) is the available energy of the canopy, ρ (kg m⁻³) is the density of dry air, C_p (J K⁻¹ kg⁻¹) is the specific heat of air, e_a (kPa) is the actual vapor pressure, e_s is the saturation vapor pressure (kPa), $VPD = e_s - e_a$ is the vapor pressure deficit, and G_a (m s⁻¹) is the aerodynamic conductance. Following the approach in Barros et al. (2019), the available energy A is assumed to be equivalent to the sum of sensible and latent heat flux. G_a is calculated with the expression in Garratt (1994):

$$G_a = \frac{ku^*}{\ln\left(\frac{z-d}{z_{om}}\right) + \Psi_H} \quad (16)$$

where u^* (m s⁻¹) is the friction velocity measured at the eddy covariance height z (41 m), d (m) is the zero plane displacement height, z_{om} (m) is the roughness length for momentum, k (-) is the von Karman's constant (0.41). Given canopy height of $h = 24.9$ m, d , and z_{om} were estimated as $d = 0.67 h$, $0.123 h$, respectively as a common practice in the absence of other information (Garratt, 1994). Ψ_H is a correction for stability conditions.

Partitioning ET into transpiration and soil evaporation is not an easy task and is still an area of active research (Stoy et al., 2019). In ecosystems with high LAI, transpiration dominates ET because leaf evaporative area greatly exceeds ground area and because little energy reaches the forest floor. Therefore, T in Equation 15 was taken from latent heat flux for this analysis. G_s was calculated using only the fluxes for local day times (6:00–18:00) when the canopy was dry (all data up to 12 h after precipitation were removed) to exclude evaporation from intercepted rainfall and minimize contribution from soil evaporation (Barros et al., 2019).

2.5.2. Estimated G_s Based on Sap Flux

Eddy covariance water flux measurements combine transpiration and evaporation, therefore the VPD effect on G_s based on the inversion method above represents a whole ecosystem level response which includes contribution from soil (Scanlon & Kustas, 2012; Wilson et al., 2001). At BCI, LAI varies between 5 and 6.5 with lower values during the dry season (Detto et al., 2018; Wirth et al., 2001). Thus, considering the large foliage evaporative area relative to the ground surface and that little energy reaches the forest floor, except for periods immediately after rainfall, the contribution of soil evaporation should be small.

In order to verify the effect of VPD on G_s without having to worry about soil evaporation, G_s was also estimated using sap flux measurements from individual trees (Ewers et al., 2001; Granier, 1987; Oren et al., 1999). The following equation was used to calculate G_s (m s⁻¹) (Ewers et al., 2001; Tang et al., 2006):

$$G_s = (115.8 + 0.4226T) \frac{J_s}{VPD} f \quad (17)$$

where J_s (kg H₂O m⁻² s⁻¹) is sap flux per unit of conducting xylem area, T (°C) is temperature, VPD (kPa) is vapor pressure deficit, $f = \frac{A_s}{A_L}$ is sapwood area to leaf area ratio (m² m⁻²), A_s [m²] is the sapwood area, and A_L [m²] is the leaf area of trees. The relations of sapwood area (cm²) to diameter at breast height (DBH) (cm) in Meinzer et al. (2001) and leaf area (m²) to sapwood area (m²) in Togashi et al. (2015) for tropical trees are used for G_s calculation in Equation 17 and they are shown below:

$$A_s = 1.582 \text{ DBH}^{1.764} \quad (18)$$

$$\log(A_L) = 1.08 \log(A_s) + 3.72 \quad (19)$$

2.6. Empirical Relationship Between G_s and VPD Under Varying Soil Moisture Conditions

The stomatal sensitivity is proportional to the magnitude of G_s when VPD is less than or equal to 1 kPa (Oren et al., 1999 and references therein). Restricting the analysis to high solar radiation ($R_s > 500 \text{ W m}^{-2}$) to minimize light effect on G_s , the relationship between G_s and VPD changes with soil moisture and is quantified using the following linear regression equation (Novick et al., 2016; Oren et al., 1999):

$$G_s = G_{s,ref} - m \times \ln(\text{VPD}) \quad (20)$$

where $G_{s,ref}$ (m s^{-1}) is a reference canopy conductance at VPD = 1 kPa. Parameter m describes the sensitivity of G_s to VPD.

To estimate the parameters in Equation 20, the hourly soil moisture data during the dry season in 2016 were first binned into quantiles defined by the 0–15th, 15th–30th, 30th–50th, 50th–70th, 70th–90th, and 90th–100th percentiles. The parameters were then determined by linear regression of G_s with the observed $\ln(\text{VPD})$ following the procedure in Novick et al. (2016). To estimate the magnitude of limitations to G_s due to soil water and VPD, we assumed the well-watered reference canopy conductance ($G_{s,ww}$) to be the average of conductance that meet two conditions: (1) soil moisture content exceeds the 90th percentile, and (2) $0.9 < \text{VPD} < 1.1$ kPa during 2016 for the eddy covariance data analysis as the estimated G_s may be influenced by soil evaporation. For the other approaches, $G_{s,ww}$ was assumed to be the maximum of those in $0.9 < \text{VPD} < 1.1$ kPa. The total limitation on G_s is calculated by subtracting each G_s predicted by Equation 20 from $G_{s,ww}$. The fraction (α_{VPD}) that limits G_s due to VPD is $m \times \ln(\text{VPD})$ divided by the total G_s limitation. The mean parameters were then reported for each bin. These processes were done for G_s estimated from the measurements and that calculated internally from the simulations.

3. Results

3.1. Seasonal Model Performance

At BCI, the monthly averaged VPD during 2013–2017 ranges from 0.25 to 0.56 kPa. The ET and GPP correlation between the simulation and the observation using HYDRO was low compared to the simulation using the heuristic approach. The root-mean-squared error (RMSE) between the simulated and observed ET is 0.26 and 0.46 mm d^{-1} for ELM and HYDRO (ensemble mean), respectively (Figure 3b). RMSE of GPP is 0.77 and 0.93 $\text{gC m}^{-2}\text{d}^{-1}$ respectively based on comparisons between the observation and the ELM simulation and the ensemble mean of HYDRO. Most of the simulations show that there are no differences in ET and GPP caused by model representations during the wet season, but all model results are biased high in ET (0.12–1.03 mm d^{-1} for the ensemble HYDRO mean) and some are biased high in GPP (0.66–1.54 $\text{gC m}^{-2}\text{d}^{-1}$ for the ensemble HYDRO mean) compared to the observations during the dry season. Model differences in ET and GPP are large in March when VPD is the highest and in April. ET and GPP have a strong response to the diversity in plant hydraulic traits in these two months as can be seen from the boxplots in Figures 3b and 3c. The maximum differences in ET and GPP during April caused by the diversity of hydraulic traits are 0.78 mm d^{-1} and 2.6 $\text{gC m}^{-2}\text{d}^{-1}$, respectively.

We calculated the average root water extraction depth using the flux weighted approach. On average, root extracts water from shallow soil depths (0.21–0.66 m) in the wet season and deeper soil depths (0.95–1.7 m) during the dry season in the HYDRO simulations (Figure 3d). On the other hand, roots extract water at a depth of 0.54 m on average from the ELM simulation during the wet season and at a depth varying between 0.54 and 0.82 m during the dry season, with the latter much shallower than that simulated by HYDRO. With plant hydraulics, model simulation of soil moisture with default soil parameters is in agreement with that converted using TDR measurements during the dry season of 2016 (Figure 4). The ELM simulation underpredicts the soil moisture in the dry season with an average of 0.21 ($\text{m}^3 \text{m}^{-3}$) compared to 0.28 ($\text{m}^3 \text{m}^{-3}$) from the observation. HYDRO results have an average of 0.27 ($\text{m}^3 \text{m}^{-3}$). The soil moisture difference caused by the diversity of plant hydraulics is small compared to that caused by model representations in the dry season. The average soil moisture predicted by the models in the wet season ranges from 0.34 to 0.36 ($\text{m}^3 \text{m}^{-3}$), which is about 10% lower than the observation of 0.43 ($\text{m}^3 \text{m}^{-3}$). None of the simulations can capture the large variability (standard deviation of 0.067 ($\text{m}^3 \text{m}^{-3}$)) in the observed soil moisture in the wet season.

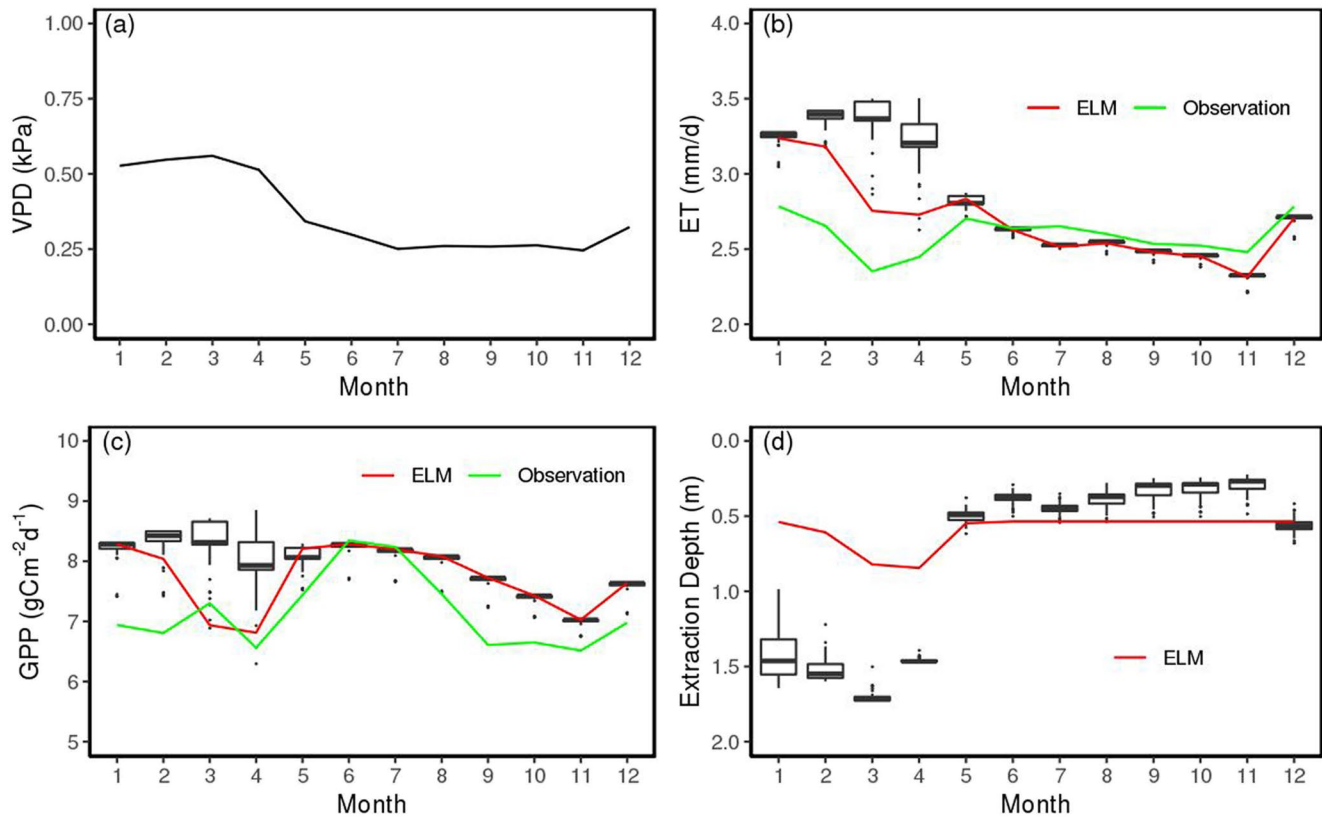


Figure 3. Seasonal change in VPD (a), ET (b), GPP (c), and average root water extraction depth (d) at BCI. All of the values were averaged overall year 2012–2016. The boxplots in (c–e) are values from the ensemble of HYDRO simulations. Boxes show the median, 25th and 75th percentiles, error bars show 10th and 90th percentiles, and filled symbols show outliers. ET, evapotranspiration; GPP, gross primary productivity; VPD, vapor pressure deficit.

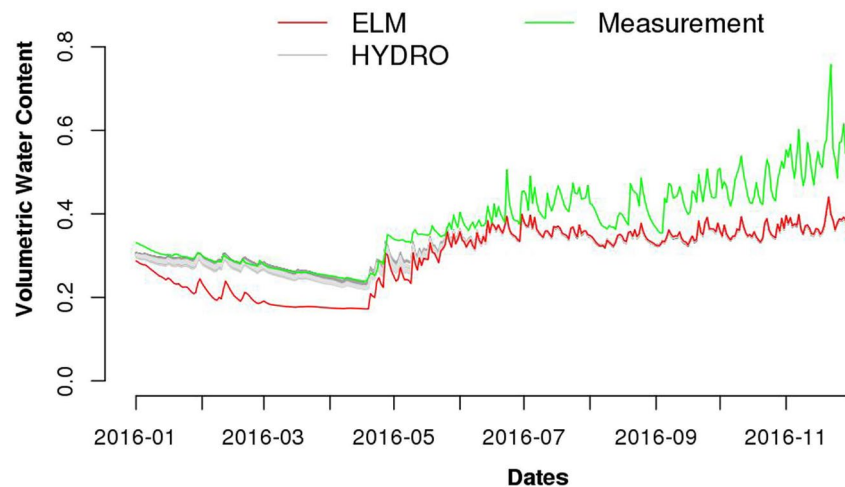


Figure 4. Comparison of simulated and measured volumetric moisture content converted from soil TDR probes at shallow soil depth (0–15 cm). The gray line indicates the range from the ensemble of HYDRO simulations, they overlap with the ELM results in the wet season. The R^2 (R-squared) and RMSE (root mean square error) for HYDRO range from 0.81 to 0.83 and 0.084 to 0.087, respectively, while R^2 and RMSE for ELM are 0.81 and 0.39, respectively. ELM, Energy Exascale Earth System Model (E3SM) Land Model; TDR, Time Domain Reflectometers.

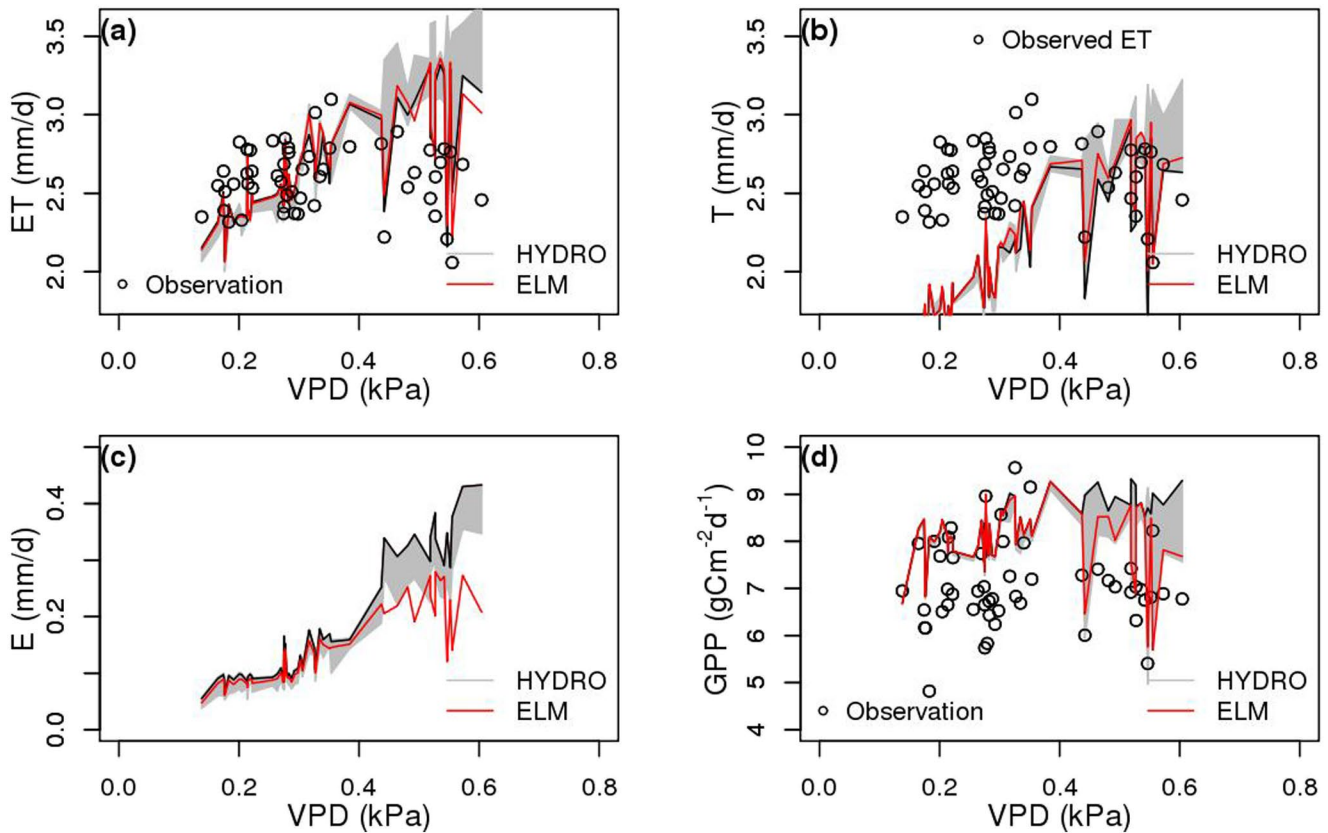


Figure 5. Response of simulated variables to VPD: Evapotranspiration (ET) (a), Transpiration (b), Evaporation (c), and GPP (d) based on monthly averages during 2013–2016. The shaded area indicates the range of the variables from the ensemble of HYDRO simulations. The black line is the HYDRO simulation with the lowest RMSE of ET and GPP, referred to as Sim37. GPP, gross primary productivity; VPD, vapor pressure deficit.

This could be due to the lack of representation of soil macroporosity, which is important in tropical forests (Bodner et al., 2013).

Plotted against monthly VPD using the results from 2013 to 2016, there is more than 10% variation in ET, transpiration (T), soil evaporation (E) and GPP (Figure 5) caused by different hydraulic traits when $VPD > 0.42$ kPa. The HYDRO simulation with the lowest RMSE of ET and GPP (the black line in Figure 5) corresponds to parameters $K_{max} = 3.96 \text{ kg MPa}^{-1} \text{ m}^{-1} \text{ s}^{-1}$, $P_{50} = -1.0 \text{ MPa}$, $a = 4$, $TLP = -0.69 \text{ MPa}$, $SA = 0.0199 \text{ m}^2 \text{ g}^{-1}$, and $WD = 0.31 \text{ g cm}^{-3}$ (a tropical species in Xu et al., 2016). It is referred to as “Sim37” hereafter. In Sim37, K_{max} is around the median, and P_{50} and TLP are the least negative among the ensemble of parameters (Figure 2). From Sim37 we can see that the simulated transpiration and GPP from ELM and HYDRO are almost identical (Figure 5). However, soil evaporation increases with the increase of VPD, and it doubles that from ELM at $VPD = 0.6$ kPa (Figure 5c). In general transpiration from model simulation plateaus while GPP decreases when $VPD > 0.4$ kPa. Relative to ELM, the larger simulated ET from HYDRO (Figure 5a) is mainly due to the larger soil evaporation (Figure 5c) from the wetter soil (Figure 4). During the dry season, the ET simulated by ELM and HYDRO are both too strong compared to the observations while the simulated transpiration alone matches the observed ET very well (note the circles in Figure 5b are observed ET, lines are T from simulations), suggesting that the simulated soil evaporation may be excessive.

3.2. Diurnal Leaf Water Potential and Sap Flux

As described in Section 2.3, leaf water potential at BCI was measured only on March 12, 2016. There were also continuous sapflow measurements during 2016. The averaged diurnal cycle of observations of leaf water potential and sapflow (averaged from four species at the site) were compared to the simulated variables

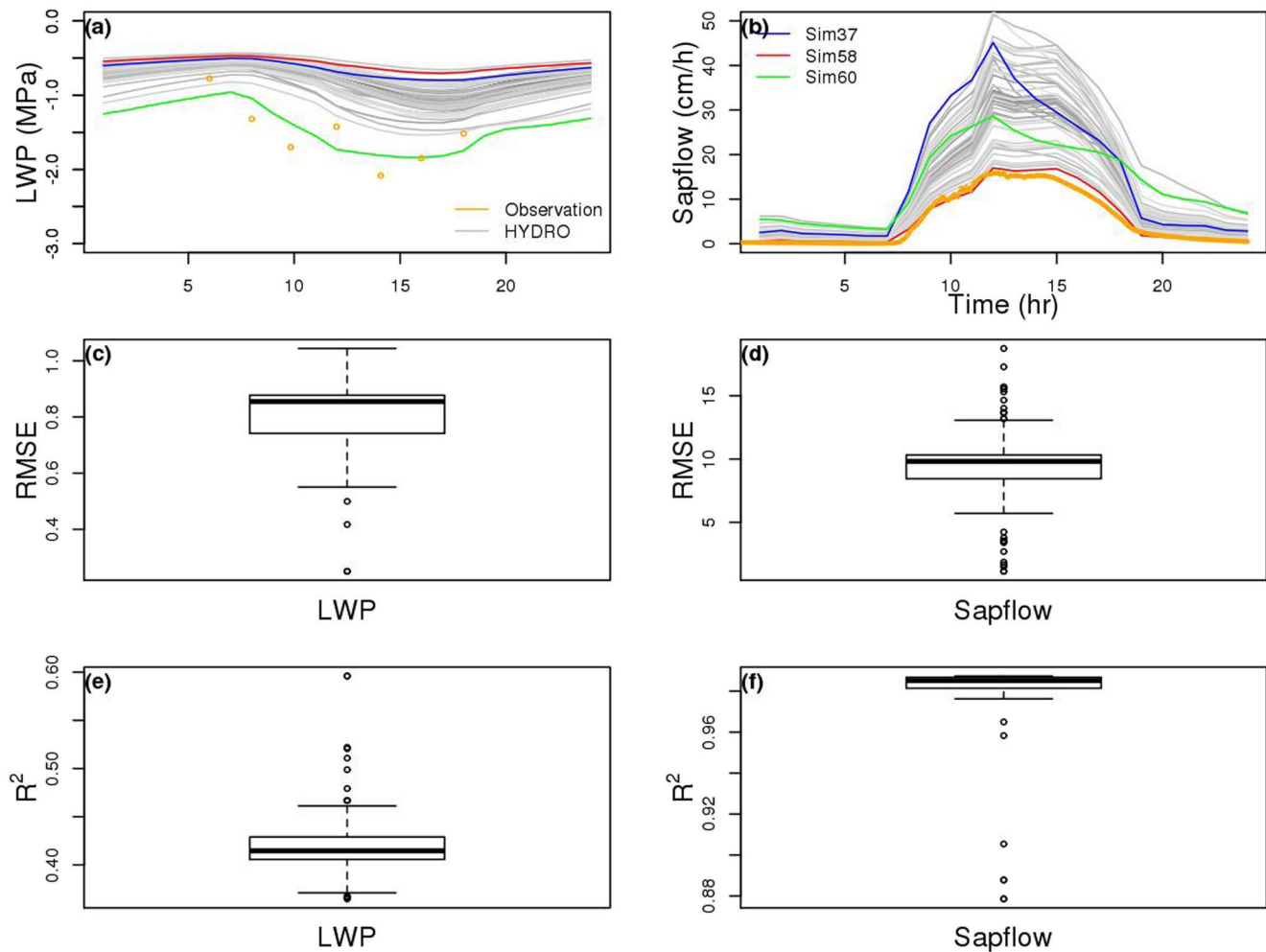


Figure 6. Diurnal cycle of measured and simulated leaf water potential (a) and sap flow (b), boxplot of the RMSE of LWP (c) and sap flux (d), and boxplot of R^2 of LWP (e) and sap flux (f) on March 12, 2016 from the ensemble of HYDRO simulations. The red line in (a and b) is the HYDRO simulation with the best performance of sap flux (Sim58) while the green line is the simulation with a better match for observed LWP (Sim60), and the blue line is the simulation with a better performance of seasonal ET and GPP (Sim37).

as shown in Figure 6. In general, the diurnal pattern of the simulations follows that of the observations. Compared to the observations: (1) the diurnal variation of leaf water potential from a majority of the HYDRO simulations is less negative (Figure 6a); and (2) the simulated sapflow is too high (Figure 6b). None of the members of the HYDRO ensemble of simulations can fully capture both the measured leaf water potential and sap flux. We note that the sapflow measurements can depend on many factors including the point where the probe is inserted if the xylem structure is irregular, the depth inside the xylem, and the reaction of the plant to the wound. Although the absolute magnitude of the flux can diverge substantially among different probes, the temporal pattern, as also predicted by most of the model simulations, remains robust.

The RMSE of leaf water potential ranges from 0.25 to 1.04 MPa (Figure 6c) and the RMSE of sap flux ranges from 1.13 to 18.73 cm h⁻¹. The R^2 between the observed LWP and the HYDRO simulations (0.36–0.60) is lower than the R^2 between the measured sap flux and the Hydro simulations which ranges from 0.88 to 0.99. Of the ensemble of HYDRO simulations, a simulation using one set of parameters ($K_{max} = 2.0$ kg MPa⁻¹m⁻¹ s⁻¹, $P_{50} = -2.12$ MPa, $a = 4$, TLP = -1.76 MPa, SA = 0.005 m² g⁻¹, and WD = 0.52 g cm⁻³) gives the best model performance for sap flux (RMSE = 1.13 cm h⁻¹) (the red line in Figure 6b). This simulation is referred to as “Sim58” hereafter. Even though one of the simulation (Sim60) with the lowest hydraulic conductance ($K_{max} = 0.16$ kg MPa⁻¹m⁻¹ s⁻¹, $P_{50} = -1.5$ MPa, $a = 4$, TLP = -1.74 MPa, SA = 0.016 m² g⁻¹, and WD = 0.77 g cm⁻³) among the ensemble of traits can better explain the diurnal magnitude of the leaf water

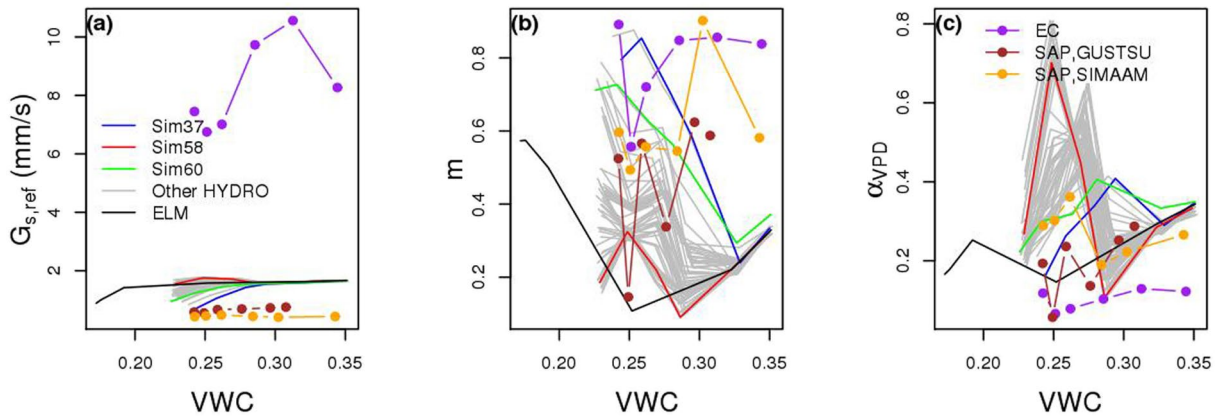


Figure 7. Regression parameter $G_{s,ref}$ (a) and m (b) for canopy conductance (G_s) as a function of vapor pressure deficit ($\ln(\text{VPD})$) and the ratio of VPD limitation to total limitation for G_s (α_{VPD}) (c), all plotted as a function of volumetric water content (VWC). Each dot represents the average value for a unique bin of VWC and VPD. The gray lines are the ensemble of HYDRO simulations. Previously identified simulations (Sim37, Sim58, and Sim60) with good performances are highlighted in color. Results from the ELM simulation are shown in black.

potential (RMSE = 0.25 MPa for Sim60, the green line Figure 6a), the simulated sap flux in the afternoon is not well correlated with the measurement. Neither of these two simulations can explain the seasonal variations of ET and GPP and the K_{max} from Sim58 and Sim60 is smaller than that ($3.96 \text{ kg MPa}^{-1} \text{ m}^{-1} \text{ s}^{-1}$) in Sim37 that best reproduced the observed ET and GPP. For ET, T, E, and GPP shown in Figure 5, Sim58 and Sim60 are at the high end of the shaded gray area (not plotted).

3.3. VPD Importance on G_s Limitation

Here the G_s limitation is estimated using the two methods described in Section 2.5.1 and 2.5.2 to evaluate the role of VPD in plant response during the 2015–2016 El Niño drought. The simulated G_s limitation is also analyzed and compared to the observation-based estimates. Using Equation 15, hourly G_s was first calculated by inverting the Penman-Monteith equation using the eddy covariance (EC) data in the dry season. The soil water content derived from the TDR measurements was binned to derive the parameters for the G_s versus VPD relationship (the purple line in Figure 7). The average parameters for the $G_s \sim \text{VPD}$ relationship is $G_{s,ref} = 8.3 \text{ mm/s}$ and $m = 0.79$. The average ratio of VPD limitation to the total limitation for G_s (α_{VPD}) was calculated as 0.1. There is no clear trend of these parameters varying with soil moisture conditions. On the other hand, the parameters derived from G_s calculated using the sap flux from two species (*Gustavia superba*, and *Simarouba amara*) exhibits smaller $G_{s,ref}$ (average of 0.55 mm s^{-1}) and m (average of 0.54) higher α_{VPD} (average of 0.23). The G_s estimated from the sap flux of *Inga Pezizifera* and *Miconia argenea* were not accounted for as the former had a lot of gaps in the data set and the latter showed no VPD limitation.

If not stated otherwise, the following comparisons are between the HYDRO simulations with better performances (Sim37, Sim58, and Sim60) and ELM. The hourly G_s data were computed internally in the model. Even though ELM simulates drier soil (black line in Figure 7) compared to the HYDRO simulations (gray lines and Sim37, Sim58, and Sim60 highlighted in blue, red, and green in Figure 7), the HYDRO simulation and the ELM simulation show decrease of $G_{s,ref}$ with soil moisture and the average $G_{s,ref}$ are comparable. Within the range of observed soil moisture, calculated average α_{VPD} for Sim37, Sim58, Sim60, and ELM are 0.3, 0.36, 0.32, and 0.24, respectively. These fractions from HYDRO are higher than those ($\alpha_{\text{VPD}} < 0.23$) calculated based on measurements, i.e., VPD has higher importance constraining G_s from model simulations than observations. Estimated parameter m and α_{VPD} from Sim37 and Sim60 are within the range of those from the observations when soil moisture is less than 0.28. α_{VPD} from ELM is comparable to those from the observations, but m is lower. VPD tends to be a dominant limiting driver for simulations with more negative P_{50} and TLP. For example, the simulation with parameters $K_{max} = 3.03 \text{ kg MPa}^{-1} \text{ m}^{-1} \text{ s}^{-1}$, $P_{50} = -3.03 \text{ MPa}$, $a = 4$, $\text{TLP} = -3.12 \text{ MPa}$, $\text{SA} = 0.006 \text{ m}^2 \text{ g}^{-1}$, and $\text{WD} = 0.8 \text{ g cm}^{-3}$.

The regression parameters vary due to the diversity of plant hydraulic traits. The average ranges of $G_{s,ref}$, m , and α_{VPD} are 1.34–1.67, 0.22–0.61, and 0.3–0.4 mm s^{-1} , respectively. Within a certain soil moisture range

(0.25–0.30), α_{VPD} is greater than 0.5, VPD as a limiting driver to G_s becomes more dominant. Among all simulations, parameter $G_{s,ref}$ is almost the lowest while m is almost the highest for Sim37 (highlighted in blue in Figure 7) that best explains the seasonal variation. The regression parameters estimated from Sim37 are comparable to those from HYDRO Sim60 (highlighted in green in Figure 7) that best explains the leaf water potential. At low soil moisture ($VWC < 0.28$), almost all HYDRO simulations have higher α_{VPD} compared to that estimated from the observations (Figure 7c). HYDRO Sim58 that matches the sap flux measurement gives a high average α_{VPD} (0.40).

4. Discussion

As the forest plot at BCI has been intensively studied, many measurements can be used for model parameterization development and evaluation. Using analysis from observations and numerical model simulations, we evaluated the relative importance of VPD as a driver for G_s limitation at BCI during the ENSO event in 2015. From the regression model derived based on observations, we found that VPD is not a dominant driver for G_s limitation at BCI. However, variations of the regression parameters derived from observations using different methods are large. Similarly, variation in the regression parameters from model simulations with different model parameter values is large. VPD is a more dominant driver for G_s limitation from the simulations than observations.

4.1. Estimated G_s and VPD Relationship From Different Observations

EC data and sap flux measurements have been commonly used to estimate G_s . When we used EC data to determine the parameter m that indicates G_s sensitivity to VPD, it was higher than the value determined from the sap flux measurements (average = 0.79 and 0.54, respectively). Despite the uncertainty in estimating G_s and m , the VPD contribution to G_s limitation is not dominant ($\alpha_{VPD} < 0.4$).

We chose the EC data when the canopy was dry (all data up to 12 h after precipitation were removed) to assume that most of the flux from EC was due to transpiration. However, sap flux (representing tree level transpiration) can only explain 60%–70% of the ET subset, i.e., not all ET from the EC data is due to transpiration only. We found the correlation between the hourly sap flux and soil water content of the top 15 cm was low ($R^2 = 0.01$) and thus they were almost decoupled emphasizing the role of water demand (VPD) on sap flow. Nevertheless, the measured soil water content can explain more than 10% of ET when combined with sap flux. These results suggest that the influence of soil evaporation was not completely removed when EC data were used to calculate G_s .

The average $G_{s,ref}$ from the EC data and sap flux are 8.3, and 0.55 mm s⁻¹, respectively. They are lower than the reported 11.8 mm/s in Granier et al. (1996) for tropical rainforest and the monthly mean $G_{s,ref}$ (~10 mm/s) in Barros et al. (2019). When EC data were used to calculate G_s , we assumed the available energy absorbed by the surface to be equivalent to the sum of sensible and latent heat flux because of the lack of measured soil heat flux. This assumption is reasonable in that it accounts for problems with flux underestimation and energy closure that are known to affect turbulent fluxes obtained from eddy covariance. Our analysis using net radiation minus soil heat flux (approximated from the GradCal approach in Liebethal et al. (2005)) as available energy in the PM equation shows underestimated G_s and lower α_{VPD} (Figure S2) compared to those using the EC fluxes. The leaf area to sapwood area ratio needs to be better quantified in order to better estimate G_s using sap flux measurements from individual trees.

4.2. Simulated G_s and VPD Relationship

As inferred from the $G_{s,ref}$ simulated by ELM and HYDRO (Figure 7a), there is no significant difference in the magnitude of $G_{s,ref}$ calculated by the model whether the stomatal sensitivity to leaf water potential is ignored or not. But the range of $G_{s,ref}$ is much lower than that from the EC data (by a factor of ~5.1 on average). When soil moisture is less than 0.28 (corresponding soil water potential of -0.09 MPa) and within the range of the observations, the sensitivity of G_s to VPD (parameter m) is relatively low using the heuristic approach compared to those estimated from the observations and most of the simulations using HYDRO. Depending on the metrics for model performance, estimated parameter m can differ significantly. m from Sim58 that better explains the measured sap flux is almost the lowest among all HYDRO simulations.

There is not a common set of hydraulic traits that can be used to explain the seasonal and diurnal measured variables. Regardless of which variables can be better explained by model simulations, VPD contribution to G_s limitation from HYDRO is relatively high compared to the estimates from the measurements. However, most simulations also indicate VPD limitation is not as important as soil water stress ($\alpha_{VPD} < 0.5$).

4.3. Model Sensitivity to the Diversity of Hydraulic Traits

Monthly ET and GPP are most sensitive to plant hydraulic traits in March and April, with ET ranged from 2.6 to 3.4 mm d⁻¹ and GPP from 6.2 to 8.8 gC m⁻² d⁻¹. Midday leaf water potential and sap flux on March 12, 2016 can vary from -1.5 to -0.75 MPa and 15 to 52 cm h⁻¹, respectively. They impact the stomatal sensitivity to VPD (average m is between 0.23 and 0.61). However, their impact on soil water content is insignificant compared to that from different model representations.

4.4. Model Performance and Future Work

Measured ET, soil moisture, leaf water potential, sap flux at BCI were used to evaluate the model performance. Compared to the observations, monthly ET were underestimated and GPP were overestimated in the wet season. In the dry season, all model simulations overestimated ET and a majority of the model simulations overestimated GPP. Simulated transpiration was higher or equal to measured ET in the dry season, which suggests there is a need for parameterization of stomatal conductance in the model. Soil evaporation simulated by HYDRO is too strong, which exacerbates total ET compared to the observation. This is no surprise as HYDRO simulated wetter soil and the soil evaporation in ELM and CLM4.5 is dependent on the top layer volumetric soil moisture (Swenson & Lawrence, 2014). A better parameterization of soil evaporation (e.g., an alternative soil resistance parameterization in Swenson & Lawrence, 2014) can be tested in the future.

Our results showed that soil moisture can be better simulated when plant hydraulic processes and hydraulic redistribution are considered in the model. The fact that none of the model simulations with different parameter values was able to capture the observed high-water content in the wet season indicates missing processes in the model, such as the change of soil characteristics due to wetting-drying cycles.

The ensemble simulations did not show a single set of hydraulic traits that can produce results matching well with the observed diurnal leaf water potential, sap flow, and seasonal ET and GPP. This could be due to the footprint spatial-temporal variability of ET from the EC tower that cannot be accounted for in the model. Another cause is that the spatial-temporal heterogeneity of soil moisture experienced by each individual tree, which is on the scale of meters, differs from that of the plot scale. As demonstrated in Baker et al. (2017), model ET could be improved if soil moisture spatial variability was accounted for in land models. This can be addressed in the future version of ELM which accounts for subgrid topographic landunits and biodiversity of trait sets interacting with other abiotic drivers.

5. Conclusion

A mechanistic plant hydraulics process model has been included in the “big-leaf” version of ELM. Observations and model simulations are used to understand the role of VPD as a driver for G_s limitation in a tropical forest site at BCI. Including plant hydraulics in land models has a noticeable effect on simulating the ET and GPP, and the average depth of plant water uptake from soil, particularly under drought conditions. Although increasing model complexity by representing plant hydraulics does not noticeably improve model performance in ET compared to the observations and ELM, the model can better explain where water is being extracted from by the roots to meet transpiration demand and allow more informed interrogation of the hydraulic process throughout the soil-plant-atmosphere continuum.

In the long dry season of 2016 caused by the strong El Niño event, G_s limitation of BCI plants was driven more by water stress than VPD, as indicated by the G_s estimates from the site eddy covariance and sap flow measurements. Model simulations also indicate a larger role of water stress than VPD in the G_s limitation, although generally the model indicates a more important role of VPD than suggested by the observations.

Despite the available data set at BCI and improvement in modeled soil moisture, model-data comparison indicates a need for more experimental and observational studies. During the dry season at BCI, seasonal ET, especially soil evaporation at VPD > 0.42 kPa, simulated using HYDRO and ELM are too strong. Both ET and GPP are more sensitive to the diversity of plant hydraulic traits than soil moisture. The fact that none of the model simulations with a wide range of model parameter values are able to match different measured variables simultaneously suggest model structural uncertainty in addition to parameter uncertainty. Hence, model-data comparison at BCI points to the need for improving parameterizations, particularly for stomatal conductance and soil evaporation, in ELM. More observation data are also needed to better constrain the plant hydraulic traits, which have significant impact on simulating ET, GPP, and the role of VPD in the G_s limitation. Furthermore, the model runs were for a single plant functional type. Biodiversity model such as the FATES demographic model should be used for the evaluations in the future.

Data Availability Statement

Observational data and data for the model are available at <http://doi.org/10.5281/zenodo.3752127>.

Acknowledgments

This work was supported by the U.S. Department of Energy Office of Biological and Environmental Research as part of the Terrestrial Ecosystem Systems program through the Next Generation Ecosystem Experiment (NGEE) Tropics project. The Center for Tropical Forest Science - Forest Global Earth Observatory (CTFS-ForestGEO) supported the flux tower research. A portion of this research was performed using PNNL Institutional Computing at Pacific Northwest National Laboratory. PNNL is operated for DOE by Battelle Memorial Institute under contract DE-AC05-76RL01830.

References

- Anderegg, W. R. L., Wolf, A., Arango-Velez, A., Choat, B., Chmura, D. J., Jansen, S., et al. (2017). Plant water potential improves prediction of empirical stomatal models. *PLoS One*, *12*(10), e0185481. <https://doi.org/10.1371/journal.pone.0185481>
- Baker, I. T., Sellers, P. J., Denning, A. S., Medina, I., Kraus, P., Haynes, K. D., & Biraud, S. C. (2017). Closing the scale gap between land surface parameterizations and GCMs with a new scheme, SiB3-Bins. *Journal of Advances in Modeling Earth Systems*, *9*, 691–711. <https://doi.org/10.1002/2016MS000764>
- Barros, F. D. V., Bittencourt, P. R., Brum, M., Restrepo-Coupe, N., Pereira, L., Teodoro, G. S., et al. (2019). Hydraulic traits explain differential responses of Amazonian forests to the 2015 El Niño-induced drought. *New Phytologist*, *223*(3), 1253–1266. <https://doi.org/10.1111/nph.15909>
- Bartlett, M. K., Detto, M., & Pacala, S. W. (2019). Predicting shifts in the functional composition of tropical forests under increased drought and CO₂ from trade-offs among plant hydraulic traits. *Ecology Letters*, *22*, 67–77. <https://doi.org/10.1111/ele.13168>
- Bodner, G., Scholl, P., & Kaul, H.-P. (2013). Field quantification of wetting-drying cycles to predict temporal changes of soil pore size distribution. *Soil and Tillage Research*, *133*, 1–9. <https://doi.org/10.1016/j.still.2013.05.006>
- Bonal, D., Burban, B., Stahl, C., Wagner, F., & Hérault, B. (2016). The response of tropical rainforests to drought—lessons from recent research and future prospects. *Annals of Forest Science*, *73*(1), 27–44. <https://doi.org/10.1007/s13595-015-0522-5>
- Burrows, S. M., Maltrud, M., Yang, X., Zhu, Q., Jeffery, N., Shi, X., et al. (2020). The DOE E3SM v1.1 biogeochemistry configuration: Description and simulated ecosystem-climate responses to historical changes in forcing. *Journal of Advances in Modeling Earth Systems*, *12*, e2019MS001766. <https://doi.org/10.1029/2019ms001766>
- Cano, I. M., Shevliakova, E., Malyshev, S., Wright, S. J., Detto, M., Pacala, S. W., et al. (2020). Allometric constraints and competition enable the simulation of size structure and carbon fluxes in a dynamic vegetation model of tropical forests (LM3PPA-TV). *Global Change Biology*, 1–17.
- Cavaleri, M. A., Coble, A. P., Ryan, M. G., Bauerle, W. L., Loescher, H. W., & Oberbauer, S. F. (2017). Tropical rainforest carbon sink declines during El Niño as a result of reduced photosynthesis and increased respiration rates. *New Phytologist*, *216*(1), 136–149. <https://doi.org/10.1111/nph.14724>
- Choat, B., Brodribb, T. J., Brodersen, C. R., Duursma, R. A., López, R., & Medlyn, B. E. (2018). Triggers of tree mortality under drought. *Nature*, *558*(7711), 531–539. <https://doi.org/10.1038/s41586-018-0240-x>
- Christoffersen, B. O., Gloor, M., Fauset, S., Fyllas, N. M., Galbraith, D. R., Baker, T. R., et al. (2016). Linking hydraulic traits to tropical forest function in a size-structured and trait-driven model (TFS v1-Hydro). *Geoscientific Model Development*, *9*(11), 4227–4255. <https://doi.org/10.5194/gmd-9-4227-2016>
- Clapp, R. B., & Hornberger, G. M. (1978). Empirical equations for some soil hydraulic properties. *Water Resources Research*, *14*(4), 601–604. <https://doi.org/10.1029/Wr014i004p0601>
- Collatz, G. J., Ball, J. T., Grivet, C., & Berry, J. A. (1991). Physiological and environmental-regulation of stomatal conductance, photosynthesis and transpiration: A model that includes a laminar boundary-layer. *Agricultural and Forest Meteorology*, *54*(2–4), 107–136. [https://doi.org/10.1016/0168-1923\(91\)90002-8](https://doi.org/10.1016/0168-1923(91)90002-8)
- Corlett, R. T. (2016). The impacts of droughts in tropical forests. *Trends in Plant Science*, *21*(7), 584–593. <https://doi.org/10.1016/j.tplants.2016.02.003>
- Daszkowska-Golec, A., & Szarejko, I. (2013). Open or close the gate—stomata action under the control of phytohormones in drought stress conditions. *Frontiers of Plant Science*, *4*, 138. <https://doi.org/10.3389/fpls.2013.00138>
- Detto, M., Baldocchi, D., & Katul, G. G. (2010). Scaling properties of biologically active scalar concentration fluctuations in the atmospheric surface layer over a managed peatland. *Boundary-Layer Meteorology*, *136*(3), 407–430. <https://doi.org/10.1007/s10546-010-9514-z>
- Detto, M., & Katul, G. G. (2007). Simplified expressions for adjusting higher-order turbulent statistics obtained from open path gas analyzers. *Boundary-Layer Meteorology*, *122*(1), 205–216. <https://doi.org/10.1007/s10546-006-9105-1>
- Detto, M., Wright, S. J., Calderón, O., & Muller-Landau, H. C. (2018). Resource acquisition and reproductive strategies of tropical forest in response to the El Niño-Southern Oscillation. *Nature Communications*, *9*, 913. <https://doi.org/10.1038/s41467-018-03306-9>
- Eller, C. B., Rowland, L., Mencuccini, M., Rosas, T., Williams, K., Harper, A., et al. (2020). Stomatal optimization based on xylem hydraulics (SOX) improves land surface model simulation of vegetation responses to climate. *New Phytologist*, *226*, 1622–1637. <https://doi.org/10.1111/nph.16419>

- Ewers, B. E., Oren, R., Phillips, N., Stromgren, M., & Linder, S. (2001). Mean canopy stomatal conductance responses to water and nutrient availabilities in *Picea abies* and *Pinus taeda*. *Tree Physiology*, *21*(12–13), 841–850. <https://doi.org/10.1093/treephys/21.12-13.841>
- Faybishenko, B., Paton, S., Powell, T., Knox, R., Pastorello, G., Varadharajan, C., et al. (2018). QA/QC-ed BCI meteorological drivers. USA. I.0. NGEET Tropics Data Collection. (dataset). <https://doi.org/10.15486/ngt/1423307>
- Fisher, R. A., Koven, C. D., Anderegg, W. R., Christoffersen, B. O., Dietze, M. C., Farrior, C. E., et al. (2018). Vegetation demographics in Earth system models: A review of progress and priorities. *Global Change Biology*, *24*(1), 35–54. <https://doi.org/10.1111/gcb.13910>
- Garratt, J. H. (1994). *The atmospheric boundary layer*. Cambridge University Press.
- Gentine, P., Green, J. K., Guérin, M., Humphrey, V., Seneviratne, S. I., Zhang, Y., & Zhou, S. (2019). Coupling between the terrestrial carbon and water cycles—a review. *Environmental Research Letters*, *14*(8), 083003. <https://doi.org/10.1088/1748-9326/ab22d6>
- Golaz, J. C., Caldwell, P. M., Van Roekel, L. P., Petersen, M. R., Tang, Q., Wolfe, J. D., et al. (2019). The DOE E3SM coupled model version 1: Overview and evaluation at standard resolution. *Journal of Advances in Modeling Earth Systems*, *11*, 2089–2129. <https://doi.org/10.1029/2018MS001603>
- Granier, A. (1985). Une nouvelle méthode pour la mesure du flux de sève brute dans le tronc des arbres. *Annals of Forest Science*, *42*, 193–200. <https://doi.org/10.1051/forest:19850204>
- Granier, A. (1987). Evaluation of transpiration in a Douglas-fir stand by means of sap flow measurements. *Tree Physiology*, *3*(4), 309–320. <https://doi.org/10.1093/treephys/3.4.309>
- Granier, A., Huc, R., & Barigah, S. T. (1996). Transpiration of natural rain forest and its dependence on climatic factors. *Agricultural and Forest Meteorology*, *78*(1–2), 19–29. [https://doi.org/10.1016/0168-1923\(95\)02252-X](https://doi.org/10.1016/0168-1923(95)02252-X)
- Green, J. K., Berry, J., Ciais, P., Zhang, Y., & Gentine, P. (2020). Amazon rainforest photosynthesis increases in response to atmospheric dryness. *Science Advances*, *6*, eabb7232. <https://doi.org/10.1126/sciadv.abb7232>
- Grossiord, C., Buckley, T. N., Cernusak, L. A., Novick, K. A., Poulter, B., Siegwolf, R. T. W., et al. (2020). Plant responses to rising vapor pressure deficit. *New Phytologist*, *226*, 1550–1566. <https://doi.org/10.1111/nph.16485>
- Hartzell, S., Bartlett, M. S., & Porporato, A. (2017). The role of plant water storage and hydraulic strategies in relation to soil moisture availability. *Plant and Soil*, *419*(1–2), 503–521. <https://doi.org/10.1007/s11104-017-3341-7>
- Haverkamp, R., & Vauclin, M. (1979). A note on estimating finite difference interblock hydraulic conductivity values for transient unsaturated flow problems. *Water Resources Research*, *15*(1), 181–187. <https://doi.org/10.1029/Wr015i001p00181>
- Huang, C.-W., Domec, J.-C., Ward, E. J., Duman, T., Manoli, G., Parolari, A. J., & Katul, G. G. (2017). The effect of plant water storage on water fluxes within the coupled soil-plant system. *New Phytologist*, *213*(3), 1093–1106. <https://doi.org/10.1111/nph.14273>
- Jackson, R. B., Canadell, J., Ehleringer, J. R., Mooney, H. A., Sala, O. E., & Schulze, E. D. (1996). A global analysis of root distributions for terrestrial biomes. *Oecologia*, *108*(3), 389–411. <https://doi.org/10.1007/Bf00333714>
- Kelleners, T. J., Seyfried, M. S., Blonquist, J. M., Bilskie, J., & Chandler, D. G. (2005). Improved interpretation of water content reflectometer measurements in soils. *Soil Science Society of America Journal*, *69*(6), 1684–1690. <https://doi.org/10.2136/sssaj2005.0023>
- Kennedy, D., Swenson, S., Oleson, K. W., Lawrence, D. M., Fisher, R., Lola da Costa, A. C., & Gentine, P. (2019). Implementing plant hydraulics in the community land model, Version 5. *Journal of Advances in Modeling Earth Systems*, *11*, 485–513. <https://doi.org/10.1029/2018MS001500>
- Kupers, S. J., Wirth, C., Engelbrecht, M. M. J., & Rüger, N. (2019). Dry season soil water potential maps of a 50 hectare tropical forest plot on Barro Colorado Island, Panama. *Scientific data*, *6*(1), 1–9. <https://doi.org/10.6084/m9.figshare.c.4372898>
- Lefsky, M. A. (2010). A global forest canopy height map from the moderate resolution imaging spectroradiometer and the geoscience laser altimeter system. *Geophysical Research Letters*, *37*, L15401. <https://doi.org/10.1029/2010gl043622>
- Lemordant, L., Gentine, P., Swann, A. S., Cook, B. I., & Scheff, J. (2018). Critical impact of vegetation physiology on the continental hydrologic cycle in response to increasing CO₂. *Proceedings of the National Academy of Sciences of the United States of America*, *115*(16), 4093–4098. <https://doi.org/10.1073/pnas.1720712115>
- Leung, L. R., Bader, D. C., Taylor, M. A., & McCoy, R. B. (2020). An introduction to the E3SM special collection: Goals, science drivers, development, and analysis. *Journal of Advances in Modeling Earth Systems*, *12*, e2019MS001821. <https://doi.org/10.1029/2019MS001821>
- Li, L., Yang, Z. L., Matheny, A. M., Zheng, H., Swenson, S. C., Lawrence, D. M., et al. (2021). Representation of plant hydraulics in the Noah-MP land surface model: Model development and multiscale evaluation. *Journal of Advances in Modeling Earth Systems*, *13*, e2020MS002214. <https://doi.org/10.1029/2020MS002214>
- Liebethal, C., Huwe, B., & Foken, T. (2005). Sensitivity analysis for two ground heat flux calculation approaches. *Agricultural and Forest Meteorology*, *132*(3–4), 253–262. <https://doi.org/10.1016/j.agrformet.2005.08.001>
- Liu, Y., Kumar, M., Katul, G. G., Feng, X., & Konings, A. G. (2020). Plant hydraulics accentuates the effect of atmospheric moisture stress on transpiration. *Nature Climate Change*, *10*(7), 691–695. <https://doi.org/10.1038/s41558-020-0781-5>
- Massmann, A., Gentine, P., & Lin, C. (2019). When Does Vapor Pressure Deficit Drive or Reduce Evapotranspiration? *Journal of Advances in Modeling Earth Systems*, *11*, 3305–3320. <https://doi.org/10.1029/2019ms001790>
- Meinzer, F. C., Goldstein, G., & Andrade, J. L. (2001). Regulation of water flux through tropical forest canopy trees: Do universal rules apply? *Tree Physiology*, *21*(1), 19–26. <https://doi.org/10.1093/treephys/21.1.19>
- Mencuccini, M., Manzoni, S., & Christoffersen, B. (2019). Modelling water fluxes in plants: from tissues to biosphere. *New Phytologist*, *222*(3), 1207–1222. <https://doi.org/10.1111/nph.15681>
- Novick, K. A., Ficklin, D. L., Stoy, P. C., Williams, C. A., Bohrer, G., Oishi, A. C., et al. (2016). The increasing importance of atmospheric demand for ecosystem water and carbon fluxes. *Nature Climate Change*, *6*(11), 1023–1027. <https://doi.org/10.1038/Nclimate3114>
- Oleson, K., Lawrence, D. M., Bonan, G. B., Drewniak, B., Huang, M., Koven, C. D., et al. (2013). *Technical description of version 4.5 of the Community Land Model (CLM)*, NCAR Tech. Note NCAR/TN-503+STR, Research, Boulder, Colorado, National Center for Atmospheric Research. Rep. (p. 420).
- Oren, R., Sperry, J. S., Katul, G. G., Pataki, D. E., Ewers, B. E., Phillips, N., & Schäfer, K. V. R. (1999). Survey and synthesis of intra- and interspecific variation in stomatal sensitivity to vapour pressure deficit. *Plant, Cell & Environment*, *22*(12), 1515–1526. <https://doi.org/10.1046/j.1365-3040.1999.00513.x>
- Osakabe, Y., Osakabe, K., Shinozaki, K., & Tran, L.-S. P. (2014). Response of plants to water stress. *Frontiers of Plant Science*, *5*, 86. <https://doi.org/10.3389/fpls.2014.00086>
- Pan, Y., Birdsey, R. A., Fang, J., Houghton, R., Kauppi, P. E., Kurz, W. A., et al. (2011). A large and persistent carbon sink in the World's forests. *Science*, *333*(6045), 988–993. <https://doi.org/10.1126/science.1201609>
- Pau, S., Detto, M., Kim, Y., & Still, C. J. (2018). Tropical forest temperature thresholds for gross primary productivity. *Ecosphere*, *9*, 1–12. <https://doi.org/10.1002/ecs2.2311>

- Phillips, N. G., Ryan, M. G., Bond, B. J., McDowell, N. G., Hinckley, T. M., & Cermak, J. (2003). Reliance on stored water increases with tree size in three species in the Pacific Northwest. *Tree Physiology*, 23(4), 237–245. <https://doi.org/10.1093/treephys/23.4.237>
- Phillips, O. L., Aragão, L. E., Lewis, S. L., Fisher, J. B., Lloyd, J., & López-González, G., et al. (2009). Drought sensitivity of the Amazon Rainforest. *Science*, 323(5919), 1344–1347. <https://doi.org/10.1126/science.1164033>
- Pineda-garcía, F., Paz, H., & Meinzer, F. C. (2013). Drought resistance in early and late secondary successional species from a tropical dry forest: The interplay between xylem resistance to embolism, sapwood water storage and leaf shedding. *Plant, Cell & Environment*, 36(2), 405–418. <https://doi.org/10.1111/j.1365-3040.2012.02582.x>
- Ricciuto, D., Sargsyan, K., & Thornton, P. (2018). The impact of parametric uncertainties on biogeochemistry in the E3SM land model. *Journal of Advances in Modeling Earth Systems*, 10, 297–319. <https://doi.org/10.1002/2017ms000962>
- Sabot, M. E. B., De Kauwe, M. G., Pitman, A. J., Medlyn, B. E., Verhoef, A., Ukkola, A. M., & Abramowitz, G. (2020). Plant profit maximization improves predictions of European forest responses to drought. *New Phytologist*, 226(6), 1638–1655. <https://doi.org/10.1111/nph.16376>
- Saito, T., Soga, K., Hoson, T., & Terashima, I. (2006). The bulk elastic modulus and the reversible properties of cell walls in developing Quercus leaves. *Plant and Cell Physiology*, 47(6), 715–725. <https://doi.org/10.1093/pcp/pcj042>
- Scanlon, T. M., & Kustas, W. P. (2012). Partitioning evapotranspiration using an eddy covariance-based technique: Improved assessment of soil moisture and land-atmosphere exchange dynamics. *Vadose Zone Journal*, 11. <https://doi.org/10.2136/vzj2012.0025>
- Sperry, J. S., & Love, D. M. (2015). What plant hydraulics can tell us about responses to climate-change droughts. *New Phytologist*, 207(1), 14–27. <https://doi.org/10.1111/nph.13354>
- Steppe, K. (2018). The potential of the tree water potential. *Tree Physiology*, 38(7), 937–940. <https://doi.org/10.1093/treephys/tpy064>
- Stocker, B. D., Zscheischler, J., Keenan, T. F., Prentice, I. C., Seneviratne, S. I., & Peñuelas, J. (2019). Drought impacts on terrestrial primary production underestimated by satellite monitoring. *Nature Geoscience*, 12(4), 264–270. <https://doi.org/10.1038/s41561-019-0318-6>
- Stoy, P. C., El-madany, T. S., Fisher, J. B., Gentine, P., Gerken, T., Good, S. P., et al. (2019). Reviews and syntheses: Turning the challenges of partitioning ecosystem evaporation and transpiration into opportunities. *Biogeosciences*, 16, 3747–3775. <https://doi.org/10.5194/bg-16-3747-2019>
- Sulman, B. N., Roman, D. T., Yi, K., Wang, L., Phillips, R. P., & Novick, K. A. (2016). High atmospheric demand for water can limit forest carbon uptake and transpiration as severely as dry soil. *Geophysical Research Letters*, 43, 9686–9695. <https://doi.org/10.1002/2016gl069416>
- Swenson, S. C., & Lawrence, D. M. (2014). Assessing a dry surface layer-based soil resistance parameterization for the community land model using GRACE and FLUXNET-MTE data. *Journal of Geophysical Research: Atmospheres*, 119, 10–299. <https://doi.org/10.1002/2014jd022314>
- Tang, J. W., Bolstad, P. V., Ewers, B. E., Desai, A. R., Davis, K. J., & Carey, E. V. (2006). Sap flux-upscaled canopy transpiration, stomatal conductance, and water use efficiency in an old growth forest in the Great Lakes region of the United States. *Journal of Geophysical Research*, 111, G02009. <https://doi.org/10.1029/2005jg000083>
- Tian, F., Wigneron, J.-P., Ciais, P., Chave, J., Ogée, J., Peñuelas, J., et al. (2018). Coupling of ecosystem-scale plant water storage and leaf phenology observed by satellite. *Nature Ecology & Evolution*, 2(9), 1428–1435. <https://doi.org/10.1038/s41559-018-0630-3>
- Togashi, H. F., Prentice, I. C., Evans, B. J., Forrester, D. I., Drake, P., Feikema, P., et al. (2015). Morphological and moisture availability controls of the leaf area-to-sapwood area ratio: analysis of measurements on Australian trees. *Ecology and Evolution*, 5(6), 1263–1270. <https://doi.org/10.1002/ece3.1344>
- Verhoef, A., & Egea, G. (2014). Modeling plant transpiration under limited soil water: Comparison of different plant and soil hydraulic parameterizations and preliminary implications for their use in land surface models. *Agricultural and Forest Meteorology*, 191, 22–32. <https://doi.org/10.1016/j.agrformet.2014.02.009>
- Vourlitis, G. L., Nogueira, J. D., Lobo, F. D., Sendall, K. M., de Paulo, S. R., Dias, C. A. A., et al. (2008). Energy balance and canopy conductance of a tropical semi-deciduous forest of the southern Amazon Basin. *Water Resources Research*, 44, W03412. <https://doi.org/10.1029/2006wr005526>
- Wilson, K. B., Hanson, P. J., Mulholland, P. J., Baldocchi, D. D., & Wullschlegel, S. D. (2001). A comparison of methods for determining forest evapotranspiration and its components: Sap-flow, soil water budget, eddy covariance and catchment water balance. *Agricultural and Forest Meteorology*, 106(2), 153–168. [https://doi.org/10.1016/S0168-1923\(00\)00199-4](https://doi.org/10.1016/S0168-1923(00)00199-4)
- Wirth, R., Weber, B., & Ryel, R. J. (2001). Spatial and temporal variability of canopy structure in a tropical moist forest. *Acta Oecologica*, 22, 235–244. [https://doi.org/10.1016/s1146-609x\(01\)01123-7](https://doi.org/10.1016/s1146-609x(01)01123-7)
- Wolfe, B., Cozzarelli, C. Y. M., & Jaén Barrios, N. (2021). *Stem hydraulic conductivity and vulnerability to cavitation for 26 tree species in Panama*. 1.0. NGEE Tropics Data Collection. (dataset). <https://doi.org/10.15486/ngt/1770723>
- Wolfe, B., Wu, J., Ely, K., Serbin, S., Rogers, A., Dickman, T., et al. (2019). *Leaf water potential, Feb2016-May2016, PA-SLZ, PA-PNM, PA-BCI: Panama*. 1.0. NGEE Tropics Data Collection. (dataset). <http://dx.doi.org/10.15486/ngt/1507766>
- Wolfe, B. T. (2017). Retention of stored water enables tropical tree saplings to survive extreme drought conditions. *Tree Physiology*, 37(4), 469–480. <https://doi.org/10.1093/treephys/tpx001>
- Wolfe, B. T., Sperry, J. S., & Kursar, T. A. (2016). Does leaf shedding protect stems from cavitation during seasonal droughts? A test of the hydraulic fuse hypothesis. *New Phytologist*, 212, 1007–1018. <https://doi.org/10.1111/nph.14087>
- Wu, J., Serbin, S. P., Ely, K. S., Wolfe, B. T., Dickman, L. T., Grossiord, C., et al. (2020). The response of stomatal conductance to seasonal drought in tropical forests. *Global Change Biology*, 26, 823–839. <https://doi.org/10.1111/gcb.14820>
- Xu, X. T., Medvigy, D., Powers, J. S., Becknell, J. M., & Guan, K. Y. (2016). Diversity in plant hydraulic traits explains seasonal and inter-annual variations of vegetation dynamics in seasonally dry tropical forests. *New Phytologist*, 212(1), 80–95. <https://doi.org/10.1111/nph.14009>
- Yuan, W., Zheng, Y., Piao, S., Ciais, P., Lombardozzi, D., Wang, Y., et al. (2019). Increased atmospheric vapor pressure deficit reduces global vegetation growth. *Science Advances*, 5(8), eaax1396. <https://doi.org/10.1126/sciadv.aax1396>
- Zhou, S., Duursma, R. A., Medlyn, B. E., Kelly, J. W. G., & Prentice, I. C. (2013). How should we model plant responses to drought? An analysis of stomatal and non-stomatal responses to water stress. *Agricultural and Forest Meteorology*, 182–183, 204–214. <https://doi.org/10.1016/j.agrformet.2013.05.009>
- Zhou, S., Williams, A. P., Berg, A. M., Cook, B. I., Zhang, Y., Hagemann, S., et al. (2019). Land-atmosphere feedbacks exacerbate concurrent soil drought and atmospheric aridity. *Proceedings of the National Academy of Sciences of the United States of America*, 116(38), 18848–18853. <https://doi.org/10.1073/pnas.1904955116>